

SUSTAINABLE WATERWHEEL TECHNOLOGY



Design Report

FEEG6013 Group Design Project

GDP 44

Kinetic Waterwheel

Designing a Floating Waterwheel for use in Irrigation Canals

Irrigation canals are an important piece of infrastructure for agriculture worldwide. They allow water to be carried to crops for irrigation in dry countries where rainfall is scarce. However, power is often required to pump this water to the fields. In rural, remote areas where mains access is limited, providing affordable sustainable energy to do this is an issue. Moreover, the flow in irrigation canals has a low energy density and thus extracting meaningful power is difficult. This project has designed and tested a novel 1:2 scale prototype for this application, the Kinetic floating waterwheel, taking the Technology Readiness Level (TRL) from 2 to 6.

This novel design extracts more power from the flow by blocking the whole width of the canal creating a head difference. This increases the available energy for extraction as both kinetic and gravitational potential energy is available.

The design was made to be both affordable and convenient. Floating means that no permanent installations are required, and the wheel can be easily moved by the consumer. Coupling this with the fact the design can be flat packed, means cheap transport and easy set-up for any location around the world.

The 1:2 scale prototype was designed and manufactured with these goals in mind and tested at the Chilworth flume facility. Several design parameters were varied including blade number and angle to obtain the optimal geometry for power generation. Experiments validated the theory behind the design, with 60 W of mechanical power extracted from a flow with available kinetic power of only 18 W.

Group Members:

ID NumberNameID NumberName31988385Samuel Hancock31742408Owain Squire31706363George Hill31907873Samuel White31861342Robert Magin

Primary Supervisor: Dr Gerald Muller Co-Supervisors: Dr Gustavo De Almeida

Submitted on: 08/05/2025

1 Contents

2	Intro	duction	2
	2.1	Increase of World's Population and Food Demand	2
	2.2	Irrigation Canals	2
	2.3	Need for Energy Production	2
	2.4	Floating Waterwheel Solution	2
3	Desig	gn Brief	3
	3.1	Stakeholder Analysis	3
	3.2	Aims & Objectives	3
4	Desig	n Process	4
	4.1	Double Diamond	4
	4.2	Triple Diamond	4
5	Litera	ature Review	6
	5.1	Waterwheels	6
	5.2	Floating Waterwheels	6
	5.3	Solar Panels	6
	5.4	Diesel Generators	7
	5.5	Hydrokinetic Turbines	7
6	Theo	ry	8
	6.1	Traditional waterwheel	8
	6.2	Floating Waterwheel	8
	6.3	Power generation	8
7	Mark	et Viability	10
	7.1	Cost Boundary Conditions	.10
	7.2	Floating Waterwheel cost calculations	10
	7.3	Backwater Curve Theory	11
	7.4	Security	11
	7.5	Decision Matrix	11
8	Desig	gn Specification	12
9	Prod	uct Lifecycle Considerations	13
	9.1	Procurement	.13
	9.2	Product Manufacturing	13
	9.3	Product use	13
	9.4	Product Disposal	13

10 Med	hanical Design	1
10.1	Channel Modifiers	1
10.2	Wheel	1
10.3	Frame	1
10.4	Ballasts / Ejection System	1
10.5	Powertrain Design	1
11 Elec	trical Design	2
11.1	System Architecture	2
11.2	Data Handling	2
11.3	Sensors	2
11.4	Power Take-off	2
12 Fina	l Prototype design	2
13 Test	Plan	2
13.1	Method	2
14 Resu	ults	2
14.1	Mechanical losses in the powertrain	2
14.2	Optimal blade number study	2
14.3	Straight Blades vs Angled for optimum blade number	2
14.4	Power Quality Graphs	2
14.5	Generator Efficiency	2

Mechanical Power Extraction26				
7 Frequency Analysis	26			
8 Audio Comparison	27			
Critical review	28			
1 Innovation	28			
2 Process	28			
3 Sustainability	28			
4 Communication	28			
urther Development	29			
1 Closed loop control	29			
2 Electrical ballast release	29			
3 Data & monitoring	29			
4 Power conversion	29			
5 Pontoon modifications	29			
References	30			
Appendix	31			
1 Appendix A	31			
2 Appendix B	32			
3 Appendix C	33			
	7 Frequency Analysis			



2 Introduction

2.1 Increase of World's Population and Food Demand

The global population is ever increasing and is set to reach almost 10 billion by 2050 [1]. This means that the world will require a predicted 56% more food to match demand compared to when the world reached a population of 7 billion in 2010 [2].

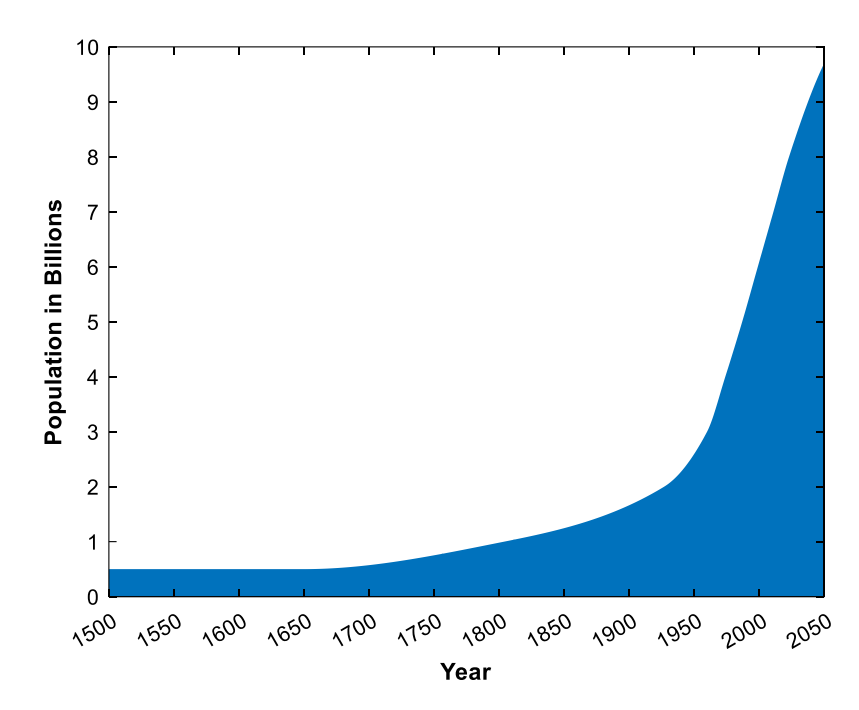


Figure 2.1 – Graph showing the evolution of global population between 1500 and projected figures in 2050 [2]

To have any chance of achieving this, it is crucial to develop technology to utilise new resources that have yet to realise their potential but are in great supply across the world, with power being a huge driver in increasing food production.

2.2 Irrigation Canals

One of the main users of the world's energy is the agricultural industry to irrigate fields. In many countries around the world, farmers use irrigation canal networks to ensure their crops are well watered. Of all global food and fodder, 40% comes from artificially irrigated fields [3]. Pumping this water currently uses around 6% of global electricity [4]. *Figure 2.2* shows the wide distribution of irrigation canals around the world.

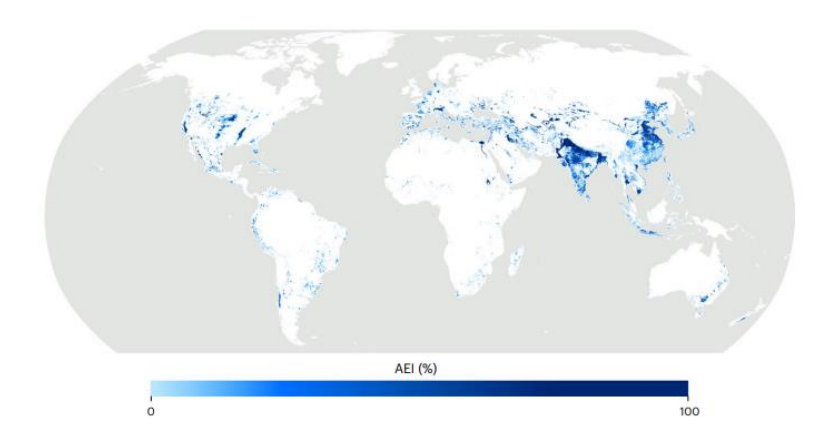


Figure 2.2 – World map with concentration of irrigation canals highlighted [5]

For example, there are more than 300,000 km of irrigation canals in India alone, and irrigation is responsible for around 70% of the world's freshwater, and as high as 90% in Spain [7][8]. As seen in *Figure 2.2*, there is a high concentration of these in developing countries like India and China, with an estimated 68% of irrigated land being in Asia [6]. This shows the potential for energy utilisation in countries with lower GDPs per capita than average, but vast populations.

2.3 Need for Energy Production

As not all irrigation canals are level or above the surrounding land, there is a need to pump water into fields as the water cannot reach the crops under gravity alone. *Figure 2.3* below shows an example of an irrigation canal located in Lliria, Spain, with this issue. The field in the background is elevated compared to the canal, with very low velocities, around 0.8 to 1.2m/s. This means a power source and energy are required to get water to the fields.



Figure 2.3 - An example of an irrigation canal where water requires pumping to the fields (Lliria, Spain)

This also means that irrigation is an untapped potential for energy usage, particularly with hydropower.

Farms in Mediterranean areas are mainly smallholdings, which are managed by older farmers with a lower level of technical education. For example, in Spain, 59% of farmers are above 55 years of age and only 18% have a high level of technical knowledge [9]. This means that a lot of energy sources that are already well established are typically out of reach to either purchase or operate for most of these farmers. They can also be very complex installations, which is incompatible for successful operation with farmers that have limited technical competencies. If irrigation technologies cannot be improved, the Mediterranean region may suffer an increase in demand of irrigation of between 4-18%, which can be interpreted as a rise of 22-74% when you start to account for population growth [10][11].

2.4 Floating Waterwheel Solution

With most of these farms and farmers being in remote rural areas, with little or no access to the mains grid, it is challenging to get energy from large-scale power stations to these areas. Thus, the easiest solution to this problem is to produce this energy locally. So far, the proposed solutions to this problem have included using diesel generators, solar panels, or traditional fixed installation waterwheels as an energy source. However, these all have their limitations regarding efficiency, power potential, cost, or a combination of all three. Given that farmers have either financial or technical knowledge limitations, a simple, low-cost, efficient product is needed to provide a more realistic solution to this need.

Therefore, this project aims to design a novel floating waterwheel that can sit in an irrigation canal and produce green, emission free power to be used for pumping water or other applications. An innovative component will be that the design blocks the canal, causing a head difference and allowing the wheel to extract more power from the low energy density flow usually found in these canals, leading to a higher efficiency. This will fill the gap in the market that farmers on low incomes need; a low-cost, long-term sustainable investment that meets their needs to generate power.

In addition, the system will also be designed so it can be flat packed, meaning it can be easily shipped around the world as a product, for self-assembly on the desired site. This is a method that has not been done before, with most solutions to off-grid power generation sold as a fixed installation rather than a mobile product. This will help farmers who have limited technical knowledge.

3 Design Brief

3.1 Stakeholder Analysis



Direct stakeholders

Indirect Stakeholders

3.2 Aims & Objectives

3.2.1 Aims

- Design an innovative floating waterwheel for low flow velocity irrigation canals that creates a head difference through blocking a significant portion of the flow thus extracting more power than is readily available.
- Achieve a design so that the waterwheel can be shipped as a flat packed kit that is easy to assemble and user-friendly to consumers with limited technical knowledge. This will fit onto regular sized euro pallets (1.2 m x 0.8 m x 2.2 m).
- Obtain a low-cost model which is accessible to consumers with low incomes.

3.2.2 Objectives

- Design and manufacture a 1:2 scale prototype of this new product that converts kinetic energy of a low velocity flow to meaningful electrical power.
- Experimentally validate the theory behind the product through testing in the Chilworth flume facility.
- Successfully design and test a safety mechanism that allows the wheel to lift out of the canal in case of an emergency.
- Experimentally investigate how both number of blades and blade angle affects the performance of the wheel to determine an optimum configuration.
- Design the prototype with a low unique part count, utilising low-cost off-the-shelf components where possible.
- Design and manufacture the prototype for an assembly process that requires a low level of technical knowledge and minimal permanent joints.
- Produce clear and concise conclusions on the performance of the prototype and how further developments could improve the final product.

4 Design Process

The Double Diamond model is a widely adopted framework in design and engineering industries. It breaks the development process into four distinct phases: Discover, Define, Develop, and Deliver, arranged within two diamond-shaped stages. Each diamond represents a process of divergence, where ideas are expanded, and convergence, where solutions are found. The model begins with a clearly defined challenge and concludes with a final outcome.

4.1 Double Diamond

In a traditional Double Diamond process (Figure 4.1) [12]:

- The first diamond focuses on understanding the problem: broad research (Discover) narrows into a specific problem definition (Define).
- The second diamond develops solutions: a wide range of ideas (Develop) are filtered down to a final solution (Deliver).
- The three circles in the diagram represent the key inputs and outputs of each stage. Each circle serves as the output of one phase and the input to the next, creating a clear, logical flow through the process. This structured progression enhances project management by highlighting dependencies and ensuring that critical tasks are completed in the desired sequence.

For this waterwheel project, the standard design process was adapted to better align with its aims and objectives. The immediate aim was to design and construct a 1:2 scale prototype, which would serve as a proof

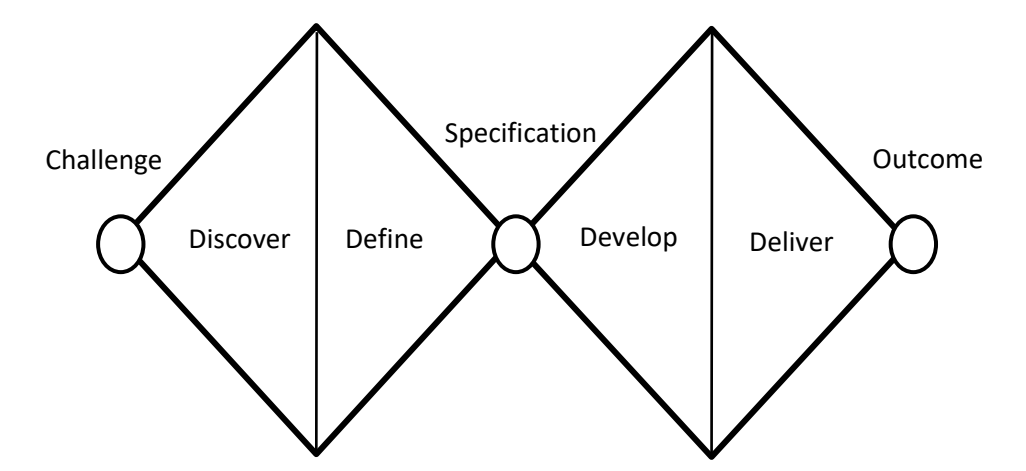


Figure 4.1 – Double Diamond Process – Design Council of concept for a future full-scale 3-metre waterwheel intended for deployment in specific irrigation canals.

The scaled prototype is therefore the practical outcome of this project but is also a product. Its purpose was to validate theoretical models and engineering calculations, as well as assess key design parameters in a controlled environment. This prototype is critical for steps towards the 3m full scale version of the system.

4.2 Triple Diamond

To accommodate this, we extended the standard model into a Triple Diamond Process (*Figure 4.2*):

 First Diamond – Research and Definition. This stage included an indepth literature review encompassing theoretical models,

- background research, market viability, and stakeholders. The goal was to fully understand the design context and establish a well-defined design specification.
- Second Diamond Design Development. Here, mechanical and electrical designs were developed in parallel, reflecting how these disciplines progressed simultaneously in practice. This stage resulted in an initial prototype design, integrating both theoretical calculations and practical considerations.
- Third Diamond Testing and Evaluation. The final stage included prototype testing, data analysis, and a comprehensive project review. This allowed for reflection on both design effectiveness and areas for improvement. The outcome of this stage was a set of "further steps" outlining potential improvements to the current design and suggestions for features or concepts that could be explored in future projects.

This adapted Triple Diamond framework maintained the core strengths of the original double diamond model, structured divergence and convergence, but tailored it to the iterative nature of prototyping and real-world testing. Moreover, the final diamond naturally led into a "further steps" section, emphasising future development that can be completed in order to create the full scale 3m version.

Each phase of this process is supported by detailed sub-sections, colour-coded and diagrammatically represented on the following page.

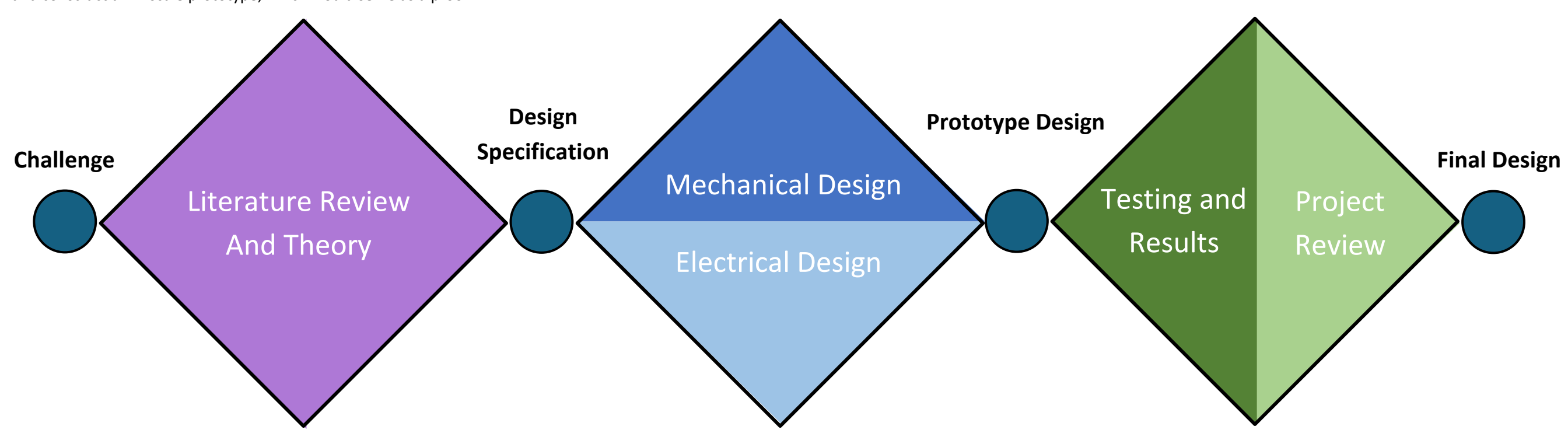
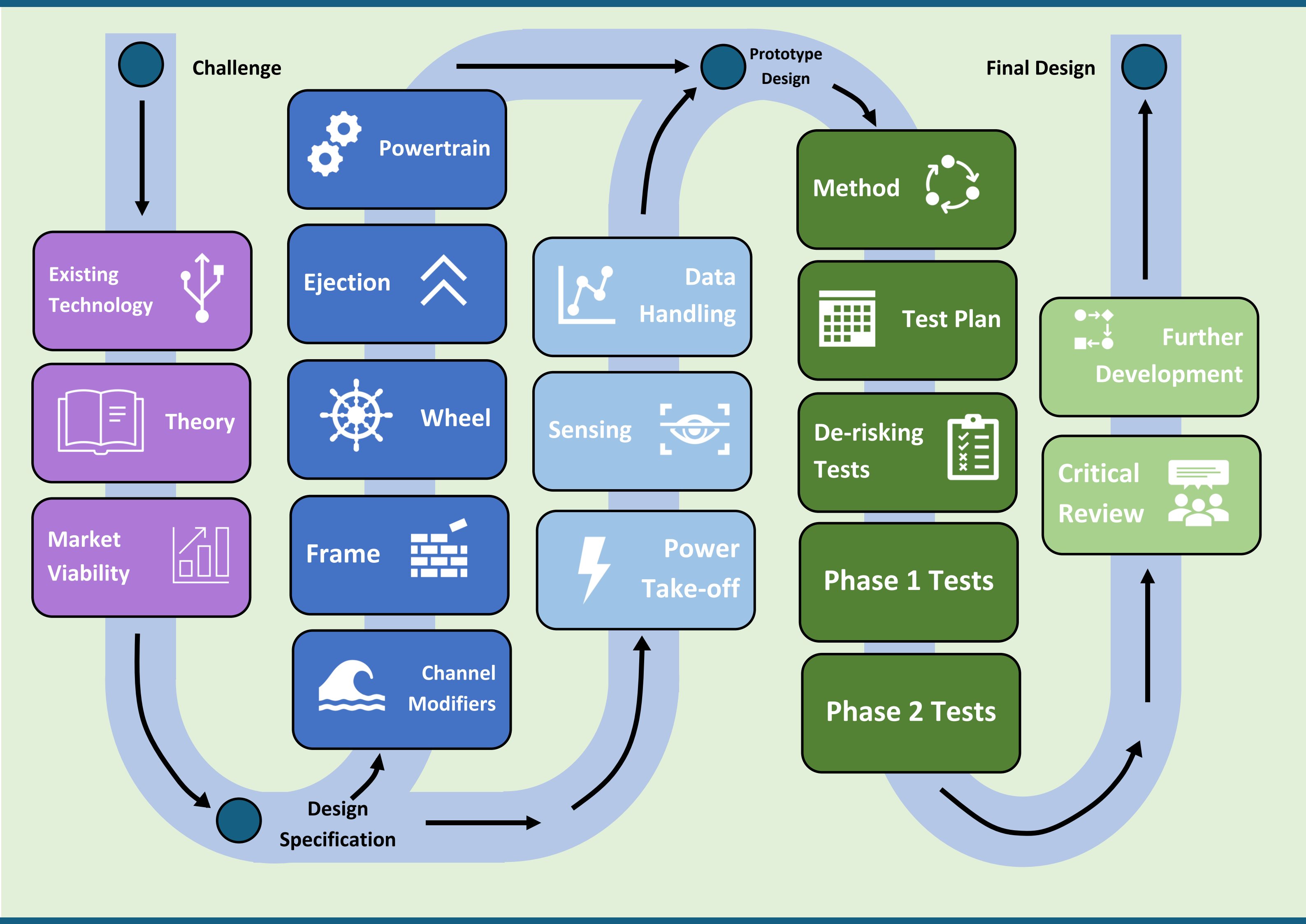


Figure 4.2 – Triple diamond design process and sections



5 Literature Review

There is a significant volume of existing technology which has been attempted to be applied to irrigation canals in an attempt to generate power. These are evaluated in this section, outlining their potential advantages and their ultimate shortcomings.

5.1 Waterwheels

Waterwheels are not a new concept; they have been used for centuries for small scale power generation [13]. There are three common types of wheel: stream (also known as undershot wheels), breastshot and overshot wheels. Stream wheels have most simple concept; the water from the river or canal is passed through the wheel, applying a force to the blades which causes the wheel to rotate.



Figure 5.1 – Example of a traditional stream waterwheel installation [14]

The reason why fixed stream waterwheels have not been used more widely as an irrigation solution is that they produce very low power and poor efficiency, a maximum of just 24% in the case of ancient watermills as seen in *Figure 5.1* [15]. This is because in most cases, they build up none or very little head difference, which means that they are only using a small percentage of the available water to extract hydropower, removing their capability to use potential energy. As flow velocities are very low in irrigation canal applications, only very low amounts of kinetic energy can be generated.

Breastshot waterwheels work differently to stream waterwheels. They operate with the water entering the wheel at a similar or slightly higher level than the wheels axle and using the gravitational potential and kinetic energy of the water to rotate the wheel and generate power. This means that they can generate an estimated 60-70% efficiency, higher than stream waterwheels [16]. The disadvantage is that they rotate at a very slow speed, and have to use drop structures, such as a weir or dam, to be able to function. This is because they cannot generate a head difference from the water by themselves instead

relying on permanent installations to do this for them. These drop structures aren't present in irrigation canals [16].

Overshot waterwheels are the current type of waterwheel that can provide the highest efficiency, around 80-85% [17]. This is because they function with water entering the wheel at its highest point, via a tube or a dam. This means that the gravitational potential energy can be utilised to its maximum, more so than breastshot waterwheels due to the magnitude of its head. The problem with these is that, due to their high head requirement, they require a bigger drop structure than breastshot wheels, which are already inappropriate for irrigation canal applications [17]. This means that their use is restricted to mountainous areas or areas with large dams, as they require head differences of 2-10 m [17]. This means that despite its high efficiency this is not a sustainable solution for an irrigation canal.

All traditional waterwheels are also fixed installations, so cannot be moved if there is a change in water level (depending on season) or if their use is required in a different site.

5.2 Floating Waterwheels

Floating waterwheels have started to be explored in recent years, due to their ability to block the canal and generate their own head difference, whilst being mobile, therefore requiring less personnel for setup and the potential for a higher efficiency due to the possibility of a higher submerged depth. First concepts of this came from a Dutch company called aQysta, an example of which can be seen in *Figure 5.2* [18].



Figure 5.2 – aQystas floating waterwheel installation [18]

Due to the relatively cheap cost to purchase and operate, this is a viable option for use in small canals. However, as *Figure 5.2* shows, the main limitation with this installation is that it takes up a very limited

space of the canal. This means the potential power it can yield is very low, giving it a very low efficiency. The application is thus restricted for either very small canals or micro-operations and is no better than the other competitors assessed when in this configuration, despite the potential.

Floating waterwheels can become very useful for irrigation if they can block a significant proportion of the flow in a canal. This would create the potential for a significant increase in head difference, thereby creating more discharge and producing more power, as well as a high efficiency.

5.3 Solar Panels

Solar panels are typically seen as the solution for green electricity generation, as they exclusively use renewable energy and do not rely on fossil fuels. They also are relatively cheap to operate, with maintenance costs typically totalling £100-200 per year, and generate green energy, not requiring any human input (therefore minimising secondary costs and environmental impacts) [19].

Despite their advantages, efficiency of solar panels is limited, typically yielding only an efficiency of 15-20% when new, which will decay over time [20]. There is also the issue that solar panels are heat sensitive, which can cause a further reduction in true power yield by as much as 25% in extreme cases [21]. Using Photovoltaics also necessitates the use of an inverter, as electricity is stored as DC and then typically used as AC. This comes with two problems. Firstly, the lifespan of a modern microinverter is shorter than the rest of the solar panel, typically around 10-15 years or 50% of a solar panel's lifespan (assuming a 20-25-year use). This means that across the lifespan of the solar panel, the inverter will require replacement, which will in turn mean multiple capital investments are required across one panel's lifespan [20].

An advantage solar panels have is that they don't produce any noise pollution. This is a problem with all other discussed technology as diesel generators make lots of noise when running and any waterwheel makes noise when the blades impact the water, causing nuisance. However, solar panels take up a lot of space where they are used due to their poor useful energy density. This means that, in the case of their use as a power source to pump water from an irrigation canal, they would require lots of surrounding land. This may not necessarily be available due to the user either not owning the land, so requiring to purchase it, or wishing to use that land for other things such as growing crops. *Figure 5.3* is a good illustration of this.



Figure 5.3 – Example of solar farm which reduces available land to irrigate [22]

Solar panels can also come with unintended consequences for third parties using the area. For example, recently in the Netherlands there have been lots of complaints from pilots flying into Amsterdam about the reflection of light solar panels that can provide potentially blinding pilots if not careful, which could make them socially unfriendly [23].

5.4 Diesel Generators

Diesel Generators are an alternative method to generate electricity from irrigation canals. They offer the advantage of having a simple design and mobility options which makes them resourceful in off-grid areas.

These are much cheaper to purchase than solar panels and take up less space [24]. They also offer the advantage of being independent of any weather, unlike solar panels which rely on sunlight.



Figure 5.4 – Example of a Diesel Generator [25]

The main drawback to diesel pumps and generators is the operational cost and overall lifespan. Operational costs are significantly higher compared to alternative methods, due to the requirement of fuel to operate the pumps. Furthermore, fuel prices are volatile, and vary country to country, so cannot be predicted, meaning that there is more reliance on external factors outside of the consumer's control. *Figure 5.5* shows this, taking a sample of six countries across the world, selected due to their use of irrigation. For comparison purposes, all prices have been converted into US dollars (\$, USD) using the conversion rate at the time of writing (November 2024).

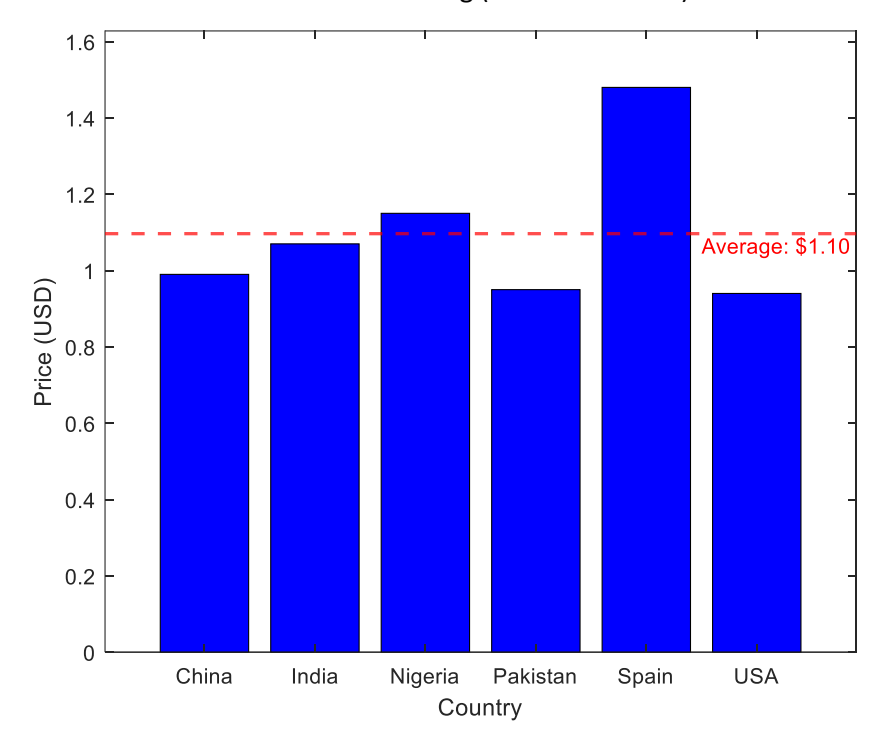


Figure 5.5 – Comparison of Average Diesel prices in countries with varying incomes and geographical location

Furthermore, diesel generators only produce a true power rating of a maximum of 50-60% of the listed power on the market. This means that to generate a desired power output, at best the true minimum investment cost will be double [26].

5.5 Hydrokinetic Turbines

Another potential method to generate electricity from irrigation canals is to use hydrokinetic turbines. These have been very successful at generating hydroelectric power in different applications, such as in large bodies of open water in oceans, where the water is very deep.

They also offer the potential of a high blockage in very narrow waterways, due to the diameter of these turbines, which enhances efficiency and making the product theoretically viable [27].

Hydrokinetic turbines do have weaknesses that are exposed in environments such as irrigation canals. Firstly, while they work well in deep waters such as oceans, the same cannot be said of shallow waters, which are typical properties of irrigation canals. These turbines do not deal very well with debris such as leaves or logs that are commonly found in such environments, which quickly accumulate in the system [27]. This means that they must be fixed in a sub-optimal position, leading to low efficiencies. *Figure 5.6* shows an example of a small-scale hydrokinetic turbine installation.



Figure 5.6 – Example of a mini-turbine installation [28]

Furthermore, although turbines over a lifespan can end up being cheaper than both diesel generators and solar panels, they have a very high initial cost, which removes low-income users from the market. They are also only able to generate low power when the flow velocity is low (anything below 1 m/s) [28]. Studies show that a minimum of 0.5 m/s flow velocity would be required to generate any power at all, ideally as high as 1.5 m/s even, whereas irrigation canals typically provide flow velocities around 1 m/s, making power generation very low [28].

Taking all this research into account, floating waterwheels have the most capacity to maximise potential energy from irrigation canals, filling this gap in the market.

The viability of floating waterwheels looks to be extensively developed by introducing novel theory highlighted below.

6 Theory

6.1 Traditional waterwheel

Firstly, it should be understood how traditional waterwheels operate in a flowing body of water. There are various ways of implementing waterwheels, as discussed above, but the following analysis will focus on the operation of a stream wheel with it being the most appropriate. This is because when operating in an irrigation canal, it is not possible to use any drop structures. The traditional stream wheel set-up can be seen in *Figure 6.1* below, where a blade is submerged in the water with a force F_1 acting upon it. This force will cause the wheel to rotate and is dictated by the velocity of the water flow and the blade dimensions. However, due to the low velocities seen in irrigation canals, there is low energy density in the flow, so it is hard to generate any meaningful power.

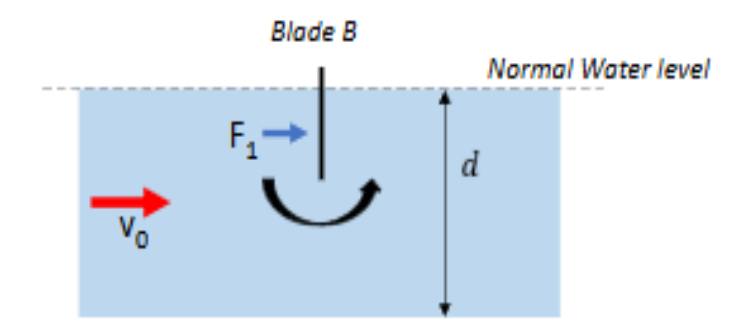


Figure 6.1 – Side view of a traditional stream wheel in a canal

Additionally, as seen in *Figure 6.1*, the blade is only partially submerged in the water and can only take up a small section of the flows cross section. This allows water to pass under or around the wheel, taking a path of least resistance, further reducing power generated. Stream wheel efficiencies can only reach a maximum of 24%, which with an already low starting energy density makes for poor power generation [15].

6.2 Floating Waterwheel

6.2.1 Novelty Aspect – Blockage and Head Difference

To improve power generation in the past, waterwheel designs have made use of drop structures, utilising the head difference between two points of a flow to extract additional power. Examples of this are overshot wheels that just use the gravitational potential energy or breastshot wheels that use both the kinetic and gravitational potential to generate power.

To overcome the low energy density problem in irrigation canals, a solution where a head difference is created by blocking the width of canal with the blades can be implemented, as seen in *Figure 6.2*.

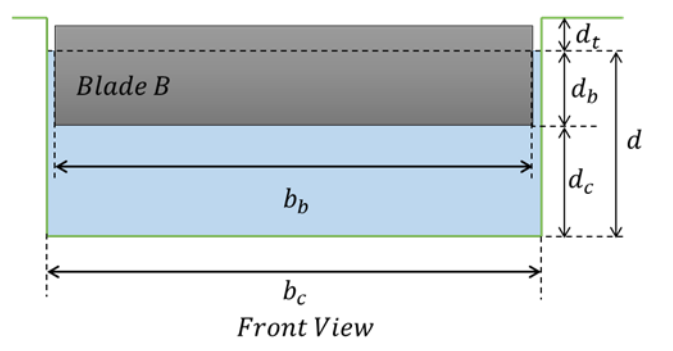


Figure 6.2 – Cross section view of canal with full wheel blockage

This setup uses the wheel to restrict the flow of water, essentially creating a blockage in the canal. This blockage will cause a small head difference to form. The wheel efficiency will thus increase greatly as both kinetic and gravitational potential energy is now extracted. As the wheel does not reach the bottom of the canal, water will be able to pass underneath, allowing for debris to flow smoothly. *Figure 6.3* shows how the introduction of a blade spanning the channel width will impact the flow.

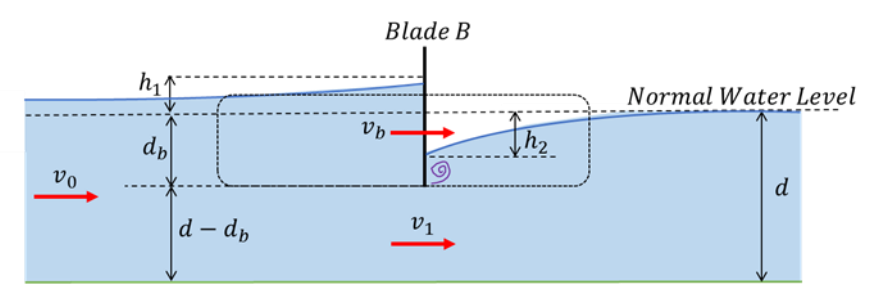


Figure 6.3 - Side view of the blade from Figure 6.2

The build-up of upstream water level caused by the blockage can be seen in *Figure 6.3*, with the level before the blade being higher than the downstream level. The blade B moves with a velocity v_b , has a submerged depth of d_b and an area of $A_b = d_b b_b$. The canal cross section area is $A_c = b_c d$. The flow through the blade is $Q_b = v_b A_b$ and the flow under the blade $Q_1 = Q - Q_b$. The velocity of the flow underneath the blades v_1 can thus be calculated using:

$$v_1 = \frac{Q_1}{A_c - A_b} > v_0$$

To calculate the head difference created by the blade, the power dissipated in the flow either side of the blade will be considered. For the upstream side, this consists of two components, the power dissipated to accelerate the flow underneath the blade and the turbulent power dissipation at the blade. These can be calculated by considering the kinetic energy of both the flow through the blade and the flow underneath. The energy transferred to the flow underneath the blade is thus a function of the difference in the two flow velocities

(V_1 - V_b). The power dissipated to accelerate the flow under the blade is thus:

$$P_{acc} = \rho Q \frac{(v_1 - v_b)^2}{2} \tag{6.1}$$

And the turbulent power dissipation at the blade where the losses are determined using a loss factor C_L , which is assumed to be 0.7.

$$P_{tur} = \rho Q C_l \frac{(v_1 - v_b)^2}{2} \tag{6.2}$$

Using the formula for head difference from power, $h_{\rm 1}$ can now be calculated.

$$h_1 = \frac{P}{\rho g Q} = \frac{P_{tur} + P_{acc}}{\rho g Q} = \frac{(1 + C_L)(v_1 - v_b)^2}{2g}$$
(6.3)

At the downstream side, the water level drops by a vertical distance h_2 due to the low-pressure zone developing in the area after the blade. This is determined by the drag force F_D on the blade. This is calculated using the known drag coefficient, $C_d = 1.2$, for an infinitely long plate [29].

$$F_D = \rho A_b C_D \frac{(v_1 - v_b)^2}{2} \tag{6.4}$$

$$P_{lost} = F_D v_b = \rho A_b C_D \frac{(v_1 - v_b)^2}{2} v_b = \rho Q_b C_D \frac{(v_1 - v_b)^2}{2}$$
 (6.5)

As the power lost is due to the drag force on the blade, the dissipated power is applied to the flow through the blade here and not the whole channel.

$$h_2 = \frac{P}{\rho g Q_h} = \frac{C_D (v_1 - v_b)^2}{2g} \tag{6.6}$$

6.3 Power generation

To calculate the predicted power of our wheel, the values for the head differences can be used with the geometry of our blades to calculate the hydrostatic force applied. The two forces are illustrated in *Figure 6.4*.

Using the equation for hydrostatic force, the forces applied on either side of the blade can be calculated

$$F_1 = \rho g \frac{d_b + h_1}{2} (d_b + h_1) b_w \tag{6.7}$$

$$F_2 = \rho g \frac{d_b - h_2}{2} (d_b - h_2) b_w \tag{6.8}$$

The power P_W generated by the wheel can be calculated using the product of hydrostatic forces F_1 and F_2 and blade velocity v_b

$$P_{w} = (F_{1} - F_{2})v_{b} = \rho g b_{w} \left(\frac{(d_{b} + h_{1})^{2}}{2} - \frac{(d_{b} - h_{2})^{2}}{2}\right)v_{b}$$
 (6.9)

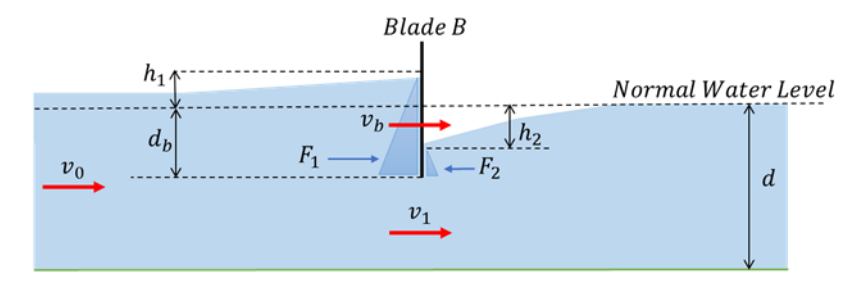


Figure 6.4 – Hydrostatic forces applied to the blade due to the head difference created

6.3.1 Pontoon effects

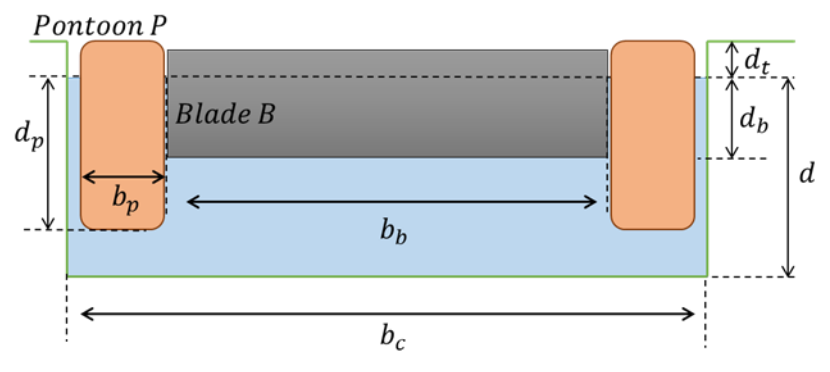


Figure 6.5 – Wheel with pontoons included

As the installation would also be using pontoons to float, the effect on the flow conditions of these being placed in the channel must be taken into consideration. The pontoons will be designed to minimise flow losses so can be assumed to have a negligible flow resistance. By introducing pontoons, the cross section of the canal will be reduced, thus increasing the local flow velocity of the channel. A cross-sectional view of the channel with pontoons can be seen in *Figure 6.5*.

For a given frontal pontoon area, A_p , the flow's new effective area becomes:

$$A_1 = A_c - A_n - A_h \tag{6.10}$$

Which changes the velocity v_1 to now equal:

$$v_1 = \frac{Q_1}{A_1} \tag{6.11}$$

With pontoons present the average velocity v_{av} over the depth range $0 \le d_i \le d_h$ is lower than the blade velocity v_h . This average velocity

can be estimated based on the assumption that the flow velocity at the pontoons is zero.

$$v_{av} = v_b \frac{b_b}{b_c} \tag{6.12}$$

This value can be used in place of v_b to recalculate the head difference h_1 (eq 6.3) with the pontoons present, and thus the new force F_1 and power generated P_W .

For h_2 , there is an additional loss due to the introduction of the pontoons, characterised here by the loss factor C_1 (again assumed to =0.7) and thus the new equation for h_2 becomes:

$$h_2 = \frac{P}{\rho g Q_b} = \frac{(1 + C_l)C_{D-}(v_1 - v_b)^2}{2g}$$
 (6.13)

6.3.2 Design optimisation

To inform design choices, the theory stated above was applied to the channel to be used for experiments. These parameters can be seen in the *Table 6.1*. The freestream velocity used here has been calculated for when the channel modifiers are in place (discussed in section 10.1) by considering the volumetric flow and the cross sections of both the Chilworth flume and the channel modifiers, with the flume flow velocity set to 0.22m/s.

Blade submerged depth and pontoon depth were also set as constant to provide enough space for any potential debris to flow underneath the blade. Blade velocity, V_b , was set to half the calculated freestream velocity V_0 , measured at the entrance to the channel modifiers.

Table 6.1 – Parameters used for design optimisation

Parameter	Value
Channel width, b _c	1.5 m
Channel depth, d	0.35 m
Blade submerged depth, d _b	0.3 m
Pontoon submerged depth, dp	0.3 m
Freestream velocity, v ₀	0.4 m/s
Blade velocity, V _b	0.2 m/s

Figure 6.6 was produced to showcase the impact of different blade widths (and thus pontoon widths) have on power. Maximum power of 60W was found for a blade width of 0.7 m. However, due to manufacturing considerations and as power only dropped slightly for a slight increase in blade width, it was decided that the blade width be 0.8m.

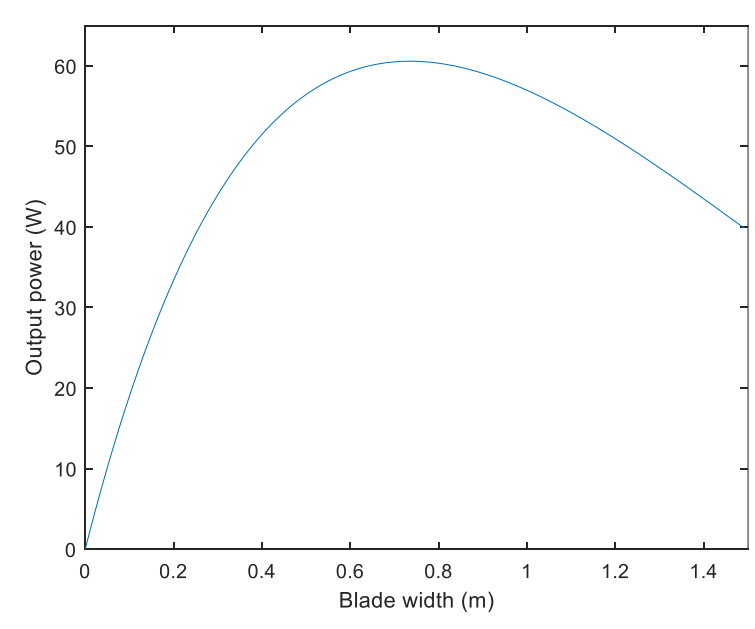


Figure 6.6 - Expected Power vs Blade width for Vb = 0.2 m/s

With this new parameter set, the power vs rpm curve for the wheel was plotted (*Figure 6.7*). This showed a maximum expected power of 59.17 W at a speed of 3.43 rpm for our waterwheel design.

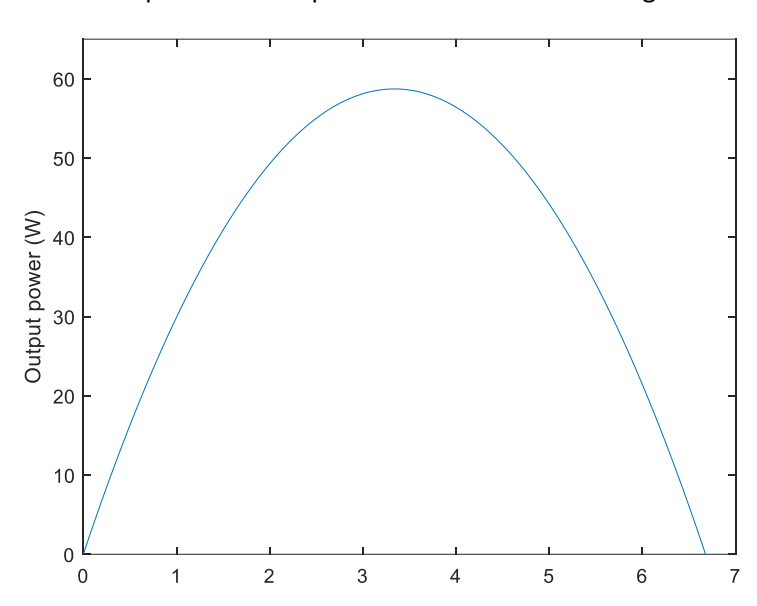


Figure 6.7 – Expected Power vs RPM for Blade width = 0.8 m

The above analysis assumes one single blade to be in contact with the water. In a real wheel, 2.5 blades should be in the water at any time. This increases the wheel efficiency. Previous research has suggested an increase by up to 50% based on a detailed numerical modelling and optimisation analysis [30]. This effect should be considered when comparing theoretical to experimental results.

7 Market Viability

For the product to be a success, it has to be competitive in the market. This section assesses the possibility of this, evaluating the costs of current existing technology and how the proposed design can be made cheaper so that it is competitive.

7.1 Cost Boundary Conditions

To determine the cost targets for the product, a cost analysis of existing technologies was undertaken in addition to the summaries given above. This was done by selecting a 5kW power rated installation for each application and comparing the costs for a 20-year usage, using the net present value (NPV) method. A 0.5% year-on-year performance degradation was applied, which is a conservative value, and for all technologies apart from solar panels a 5000-hour yearly use was assumed. *Table 7.1* shows the list of parameters used for all calculations:

Table 7.1 – Cost calculations parameters [24][31]

Parameter	Solar	Diesel	Turbines	Wheel
NPV Discount Rate (%)	5	5	5	5
Initial Investment Cost (£)	55,700	1,335	25,000	10,200
Yr-on-Yr Performance Degradation (%)	0.5	0.5	0.5	0.5
Annual use (h)	5,000	5,000	5,000	5,000
Annual Operational Costs (£)	200	13,500	2,200	100
Efficiency (%)	20	30	20	80

Assumptions:

- Solar Assume 12 hrs of generation per 24 hr cycle. Requires battery replacement after 10 years and inverter replacement after 12 years at a cost of £34,500. Battery is required to get up to the 5000h of use given energy needs to be stored for overnight usage.
- Diesel 10% secondary cost added, to account for user having to travel frequently to site to refuel generator.
- Waterwheel 3 m canal width, submerged depth 0.6 m, 2 m blade width. Replacement required after 10 years.

NPV is defined as the difference between current cash inflows and future cash outflows, and is defined below, where t represents time in years, R_t represents cash flow required at time t, R_0 is the initial investment cost (expressed as a negative number), and i is the discount rate:

$$NPV = \frac{R_{\rm t}}{[(1+i)]^t} - R_0 \tag{7.1}$$

The most valuable way to display this for comparative purposes was as a cost per kWh. The assumed total lifetime energy generated for solar panels, diesel generators and turbines were taken as 100,000, 150,000 and 100,000 kWh respectively. This was calculated by taking the output power, multiplying by the efficiency, and the hours used per year, applying the performance degradation year on year accordingly. Using these and dividing by the total capital cost gives the cost per kWh target that the proposed design should be under. The overall estimated cost per kWh is given in *Figure 7.1*. For comparison purposes the national grid average cost per kWh over the last 12 months was inserted.

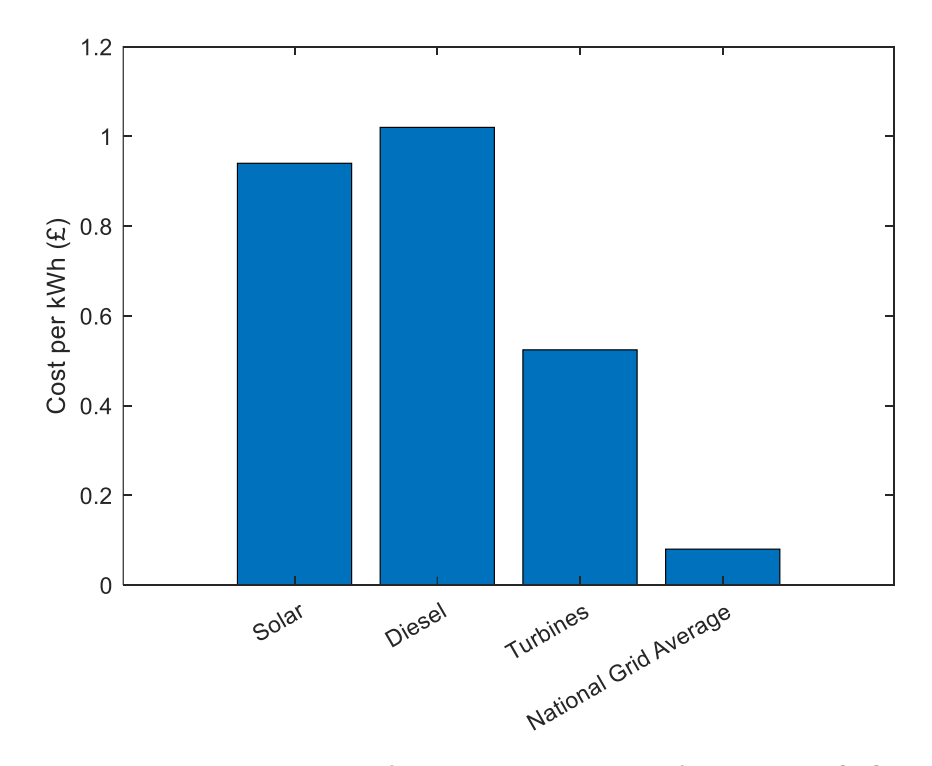


Figure 7.1 – Comparison of Energy Sources in terms of cost per kWh [32]

From this graph, it is clear on all counts that the most competitive technology from a cost perspective is the hydrokinetic turbine, with a cost of £0.26/kWh. Therefore, the requirement is to design the wheel so that the cost per kWh is below £0.52, so that it can be a competitive product.

7.2 Floating Waterwheel cost calculations

The project's budget of £1,850 facilitated the manufacturing of a 1:2 scale model. This sum included provisions for excess costs and the procurement of most materials at individual retail prices.

7.2.1 Excess Costs

Due to most orders being small-scale, a lot of fixed costs such as delivery were incurred. The other excess cost was the cost of materials

used to build the channel modifiers. *Table 7.2* gives a summary of excess costs associated with building a singular scale prototype.

Table 7.2 – Summary of excess fixed costs excluded

Excess Costs	Potential Savings (£)
Channel Modifiers Materials	314
Delivery Costs	196
Total	510

7.2.2 Bulk Discounts

Transitioning from the 1:2 scale model to full-scale mass production will naturally require a significant increase in material procurement. However, the large volumes of materials needed for mass production directly enable cost efficiencies through economies of scale, such as bulk purchasing discounts. Therefore, the material cost per unit during mass production will be considerably more favourable than initial single unit purchases.

Table 7.3 illustrates this with specific examples of savings achieved on materials for this project when comparing individual versus bulk pricing. RS Components was used as an example supplier.

Table 7.3 – Examples of savings that can be made using bulk discount – RS [33]

Component	Single cost (£)	Bulk Price (£)	Bulk Discount (%)
Plywood Sheets	38.16	29.98	21.44
Timing Belt	38.05	32.31	15.09
Arduino	16.6	14.63	13.46
Average %	N/A	N/A	16.66

Based on this estimation, the scale model material cost was £1,200 excluding the excess costs highlighted in *Table 7.2*, and an upscaled cost of £8,000.

7.2.3 Transport Costs

This product is specifically engineered for flat-pack assembly, facilitating its loading onto industry-standard Euro pallets for ease of handling and storage. The ultimate cost of transporting these palletised goods as freight is not fixed; rather, it depends significantly on the specifics of the destination. Key determinants of this cost include the geographical distance the pallet must cover and the chosen method of conveyance (e.g., truck, ship, or potentially a combination). Given that a primary design objective is to achieve the lowest possible overall cost, the transportation strategy prioritises either road or sea freight, as these are typically the most economical options for larger consignments. For a concrete financial reference point, a transportation quote was calculated using the product's specific dimensions. This quote, for shipment from Southampton to Granada, provided a baseline figure of £518 [34].

The costs above total an estimation of around £8,500 to manufacture in bulk and ship the product to customers. Given that this is a prediction and there are likely to be additional costs in the early stages of development that are either unforeseen or underappreciated here, along with market volatility particularly with shipping costs and the necessity to generate profit for a business to be viable, a 20% markup was applied. This led to a sale price for this wheel of £10,200.

Table 7.4 shows the results of the simulation of the parameters below, giving the total power generation for its lifespan. It also provides the cost per kWh and the 20-year NPV. Also inserted is the maximum allowable sale price for the wheel to remain cheaper than turbines.

Table 7.4 – Results of upscaled power and subsequent cost calculations

Parameter	Value
Power Generated (W)	1960
20-year Power Production considering Power degradation (kWh)	186000
20-year NPV (£)	17800
Cost per kWh (£)	0.10
Maximum Permitted Sale Cost to Remain Cheaper than Competitors (£)	55,000

7.3 Backwater Curve Theory

When a head difference is created, it generates a backwater curve, which means that the upstream water level remains higher than usual and tapers off asymptotically. This is important to understand as the waterwheel cannot be placed in a canal when this curve is prominent, as it will either compromise head difference generation from the wheel placed within it, or flood the canal, affecting residents.

7.3.1 Calculation of Backwater Curve

As the backwater is asymptotic, the water level never fully returns to its true original level. However, if the water level returns within 1% of its normal level, it has a negligible effect on the power or head difference. This 1% value is very conservative, with the likelihood being that the water level can be judged as 'normal' even before this point. The backwater curve profile can be calculated from Bernoulli's equation below, utilising a standard step method to work back upstream from the installation.

$$h_1 + z_1 + \frac{v_1^2}{2g} = h_2 + z_2 + \frac{v_2^2}{2g} + S_f dx$$
 (7.2)

Figure 7.2 shows a typical backwater curve profile, and the point where the water level returns to within 1% of the nominal depth. This curve was calculated for a typical canal gradient of 0.0015, normal water depth of 1m and a head increase of 0.1 m at the installation.

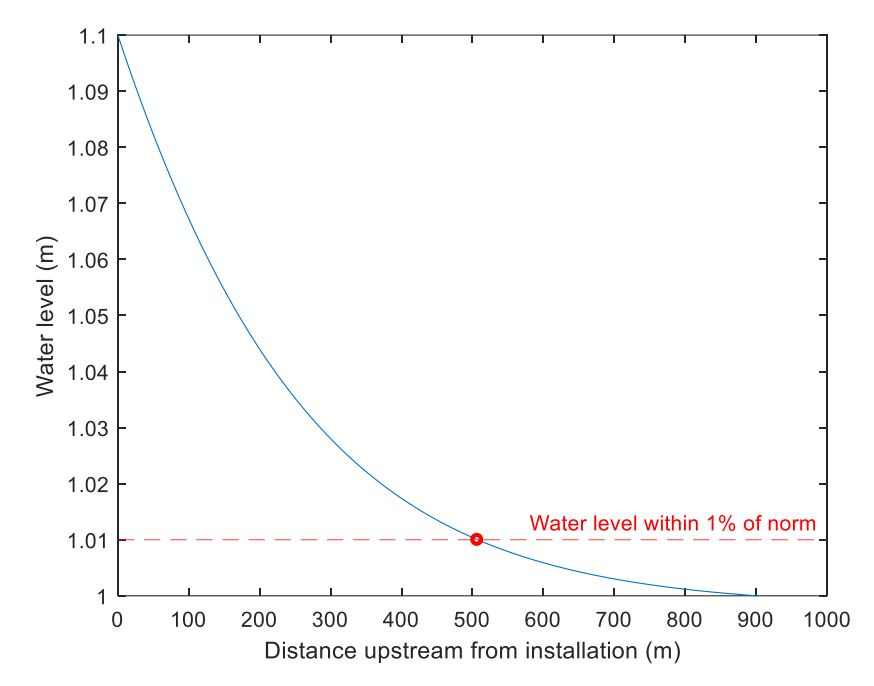


Figure 7.2 – Example of a 1000 m long backwater curve profile

7.3.2 Effect of Canal Gradient on Backwater Curve

Canal gradients are a key variable with respect to backwater curve length, which cannot be controlled, unlike the head difference. The gradient of irrigation canals can vary from 0.0002-0.0015. This may appear small but can have a big effect on the backwater curve length. *Figure 7.3* shows the length of the backwater curve for the water level to return to normal (within 1%) for varying canal gradients. This assumes a head difference of 0.1 m.

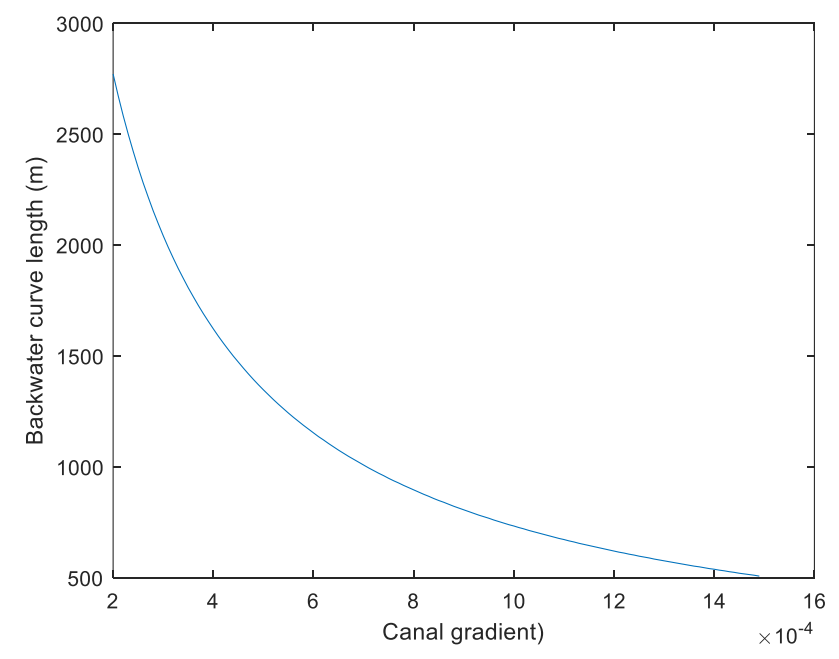


Figure 7.3 – Illustration of the effect canal gradient has on the backwater curve

7.3.3 Possible number of installations

Using the information from *Figure 7.3*, the number of installations for a set length of canal can be calculated. Depending on gradient, between 3 and 20 waterwheels can be fitted per 10 km of canal, if they are all run at maximum power. This shows that farmers can realistically buy multiple of these products without the risk of compromising power per unit, unless their canal gradient is very shallow. It also shows that neighbouring farmers who might share a canal aren't adversely affected if both wish to own the wheel further adding to the marketability of the product.

7.4 Security

From a security perspective, the assessment found that substantial installations like the proposed waterwheel and solar panels are inherently less vulnerable to theft and vandalism. Diesel generators, however, are considered easier targets due to their smaller, portable nature. Turbines were determined to have a moderate level of vulnerability, falling between these extremes, which explains their amber classification.

7.5 Decision Matrix

Table 7.5 presents a decision matrix that compares various microhydropower technologies, including a proposed design and competing options, based on critical success criteria. Each technology's performance against these criteria is visually graded using colour-coded cells: red signifies an unfavourable rating, amber indicates moderate performance, and green denotes a highly favourable assessment.

Table 7.5 – Decision Matrix comparing waterwheel design and competitors

Criteria	Wheel	Solar Panels	Diesel Generator	Turbines
Installation Cost				
Operational Cost				
Environmental Impact				
Security				

8 Design Specification

The project brief and literature review allowed us to put together a detailed specification covering the full spectrum of performance of the wheel. The design specification provided the basis for decisions moving forward and allowed the team to work synchronously to ensure all elements of the final proposal were aligned. The prototype column highlights features intended for the prototype build. The product column indicates features intended to be included in further developments of the full-scale product. **Shall** = necessary. **Should** = desirable but non-critical. **Could** = nice to have.

Table 8.1 – Project design specification

Water the all requirements						
Waterwheel requirements						
Specification	Shall Should Could	Prototype	Product	Rationale		
High level						
Generate power from an irrigation canal	Shall	Υ	Υ	Allow the user to power off grid farming equipment, e.g. pumps.		
Assembled by two people with simple tools	Shall	Υ	Υ	Facilitates installation in remote locations with limited personnel and equipment. Reduces installation cost and complexity.		
Detect and avoid blockages and flooding of the canal	Shall	Υ	Υ	Ensures operational reliability and prevents damage to the device and the canal infrastructure.		
Requires no physical connection to the channel, other than mooring lines	Shall	Υ	Υ	Minimises impact on existing canal structure, simplifies installation, and potentially avoids complex permits.		
Components are packed small with minimal voids	Shall	Υ	Υ	Optimises logistics and reduces shipping costs, especially to remote or difficult to reach sites.		
Assembly instructions that require little mechanical experience	Shall	N	Υ	Enables assembly by non-specialist users, increasing accessibility and reducing installation labour costs.		
Lifespan of >10 years	Should	N	Υ	Ensures a reasonable return on investment and reduces the long-term cost of ownership.		
Materials delivery & assembly to cost less than a similar performance competitor	Should	N	Υ	Key competitive differentiator and critical factor for market viability, especially in cost-sensitive applications.		
Performance		-	•			
Generate power at a range of flow velocities (0.05 m/s to 1.5 m/s)	Should	Υ	Υ	Defines the expected operational range, ensuring the device is effective across typical irrigation canal flow conditions.		
Adjustable to fit the width of the installation channel (2 m to 8 m)	Should	N	Υ	Allows deployment in a wide variety of common canal sizes, increasing market applicability.		
Adjustable to fit the depth of the installation channel (0.2 m to 2 m)	Should	N	Υ	Accommodates varying water levels and canal depths, ensuring optimal immersion and performance.		
Cost						
Cost less, including shipping, installation and maintenance, than a solar	Should	N	Υ	Establishes a key economic benchmark and value proposition against a common alternative renewable energy source for remote		
installation				applications.		
Cost less, including shipping, installation and maintenance, than a diesel	Should	N	Υ	Provides a competitive advantage against fossil fuel alternatives, highlighting both economic and environmental benefits.		
installation				a contract from a magnetic field and an exp. g. g. c. g. contract from a magnetic field and a		
Produce power at less than £0.26 per kWh averaged over its lifespan	Should	N	Υ	To be competitive with other solutions in the market, over its lifespan the wheel should perform to this cost per kWh.		
Form factor						
Blade submerged depth should be ½ of radius	Should	Υ	Υ	Research indicates for the most efficient performance in our flow condition range, 1:2 blade submerged depth to radius is most efficient. [35]		
When disassembled, fit on one standard size euro pallet	Should	Υ	N	Facilitates standardised, cost-effective transport and handling using common logistics infrastructure, reducing costs.		
Assembly				gggggggg		
Use standard hardware and standard tools	Shall	Υ	Υ	Simplifies assembly and maintenance, reduces the need for specialised tools, and ensures easy replacement of fasteners if needed.		
Have low unique part count (<100)	Shall	Y	Y	Reduces manufacturing complexity, simplifies inventory management, and makes maintenance/repairs easier.		
Material				ger years grant gr		
Use compatible metals for corrosion resistance	Should	N	Υ	Ensures durability and longevity in a constantly wet environment, preventing premature failure due to corrosion.		
No risk of fatigue failure in the lifespan, in normal operating conditions	Should	Y	Y	Guarantees structural integrity over the intended lifespan under normal operating loads and cycles. Critical for reliability.		
Withstand constant nominal UV exposure without affecting performance	Should	N	Y	Ensures materials exposed to sunlight do not degrade prematurely, maintaining structural integrity and performance over the lifespan.		
Blockage avoidance				g		
Reduce draught by at least 50% when ejected vs submerged	Should	Υ	Υ	Safety feature to prevent grounding or damage when the blockage avoidance system activates, allowing the device to float higher.		
Go from fully operational to fully ejected in < 3 min	Should	Y	Y	Ensures a quick reaction to potential blockage events, minimising the risk of damage to the device or canal.		
Instructions	Oriodia			Endured a quiek reaction to peterial blookage events, minimining the next of damage to the device of daman.		
Language agnostic instruction manual	Should	N	Υ	Maximises usability across different regions and user languages through clear diagrams and symbols, reducing translation needs.		
Telemetry	Oriodia			maximises dealing deress and on regions and deer languages anough seal alagrants and symbols, reducing nariotation results.		
Measure and record rotational speed of the wheel	Shall	Υ	Υ	Fundamental parameter for monitoring wheel performance and diagnosing potential issues.		
Measure and record power produced by the generator	Shall	· V	Ÿ	Directly measures the primary output and value proposition of the device. Essential for performance tracking and validation.		
Save data locally	Shall	Y	Ý	Ensures data retention even if remote communication fails. Allows for later retrieval and analysis.		
Data sampling rate at least 1 Hz	Shall	· V	Ý	Provides adequate temporal resolution for analysing dynamic performance characteristics and detecting transient events.		
Broadcast data wirelessly to nearby users	Should	· V	V	Enables convenient local monitoring and diagnostics using common devices like smartphones or tablets without physical connection.		
Measure and record pitch of the wheel	Should	\ \	N	Provides insight into the wheel's orientation and stability, useful for performance analysis and troubleshooting. (De-scoped for Product).		
Measure and record voltage produced by the generator	Should	\ \	N.	Essential parameter for monitoring the generator's electrical output and diagnosing electrical system health. (De-scoped for Product).		
Measure and record current produced by the generator	Should	V	N	Complements voltage measurement for a complete picture of electrical power output and system health. (De-scoped for Product).		
Measure and record torque at the input shaft of the generator	Should	V	N N	Allows direct measurement of mechanical power transfer, useful for efficiency calculations and diagnostics. (De-scoped for Product).		
	Shall	N	V	Critical for deployment in off-grid, remote locations typical for irrigation canals. Ensures self-sufficiency.		
Operate independently of mains connection		N	V			
Broadcast data wirelessly to global users	Should	IN V	T V	Enables remote performance monitoring, data aggregation, fleet management, and potentially remote diagnostics/control.		
Measure and record local environmental wind	Should	N	Y	Provides contextual environmental data that might influence performance or be useful for broader environmental monitoring.		
Measure and record local environmental temperature	Should	IN N	Y	Provides contextual environmental data; temperature can affect material properties and electronic performance.		
Measure and record local environmental rainfall	Could	N	Y	Provides contextual environmental data; rainfall can correlate with canal flow rates. (Lower priority).		
Connect to existing internet of things (IoT) network	Could	IN	Υ	Connecting to water pumps could allow for better power sharing & decision making on power use.		

9 Product Lifecycle Considerations

Throughout the design process, the environmental and social impacts were consistently evaluated, striving to minimise any negative effects while maximising opportunities for positive change. *Figure 9.2* presents a broad overview of the various stages of the product's lifecycle that were examined.

9.1 Procurement

During the selection of materials for the product, emphasis was placed on renewable and sustainable options, thereby minimising the environmental impact associated with their extraction and processing. Furthermore, materials that are both common and widely available were prioritised to ensure accessibility and to enhance the feasibility of production across various locations. The widespread availability of these materials reduces the need for long-distance transportation, thus mitigating the associated environmental footprint. Additionally, the ability to source materials nearby not only supports local economies but also generates social benefits. This approach further enhances the flexibility of future supply chains, as it reduces reliance on a single supplier for specialised resources.

9.2 Product Manufacturing

A key element of the project's design philosophy was the prioritisation of efficient transportation, which directly informed the decision to create a flat-packable structure. This design choice offers significant advantages from an environmental perspective by streamlining logistics and minimising the volume occupied during transit, thereby reducing the carbon footprint associated with transportation. Moreover, the selection of readily available, off-the-shelf machined parts produced through bulk manufacturing processes reduces production impacts and, similarly, transportation costs.

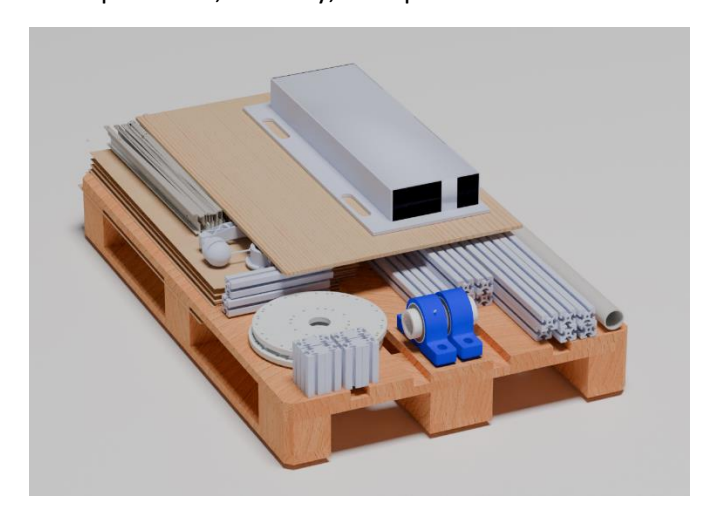


Figure 9.1 - Design Flat-packed onto a euro pallet

Figure 9.1 provides an example of the final design packed onto one euro pallet ready for transportation.

Beyond these material and logistical considerations, the flatpack design also minimises the necessity for extensive onsite construction. This objective was achieved by engineering the wheel to require only mooring points, significantly reducing the need for extensive foundation work and the associated disturbance to the surrounding environment. This simplified installation process not only lessens the impact on local ecosystems but also potentially reduces the time and resources required for deployment.

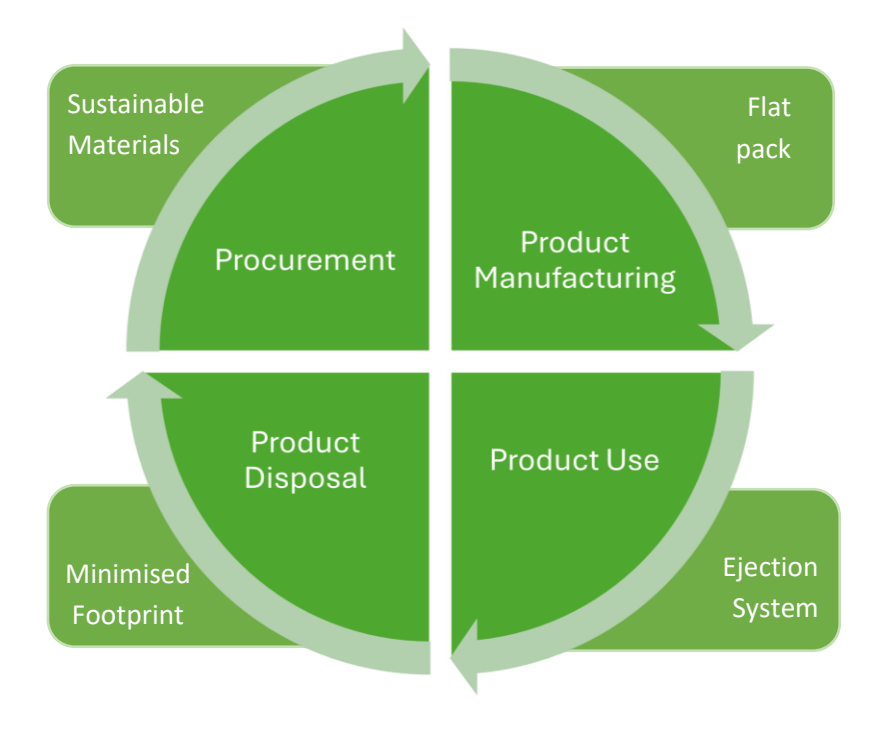


Figure 9.2 – Waterwheel product lifecycle stages

9.3 Product use

One of the key social considerations addressed during the design of the waterwheel was the potential noise generated by the impact of the blades on the water surface. Given that the intended operational environments are predominantly rural, with low ambient noise levels and minimal natural sound barriers, the propagation of sound is expected to be significant. Consequently, if the waterwheels are installed in proximity to local communities or rural dwellings, the resulting noise could pose a considerable disturbance. To mitigate this issue, the design process will incorporate specific modifications to the blade geometry aimed at reducing noise generation during operation.

The potential for upstream blockages in the canal poses a significant risk to both downstream agricultural communities and local ecosystems. Blocked water flow could lead to flooding upstream and

water deprivation downstream, impacting farmland and threatening the delicate balance of wildlife habitats. To address this critical concern and ensure the consistent flow of water, the wheel's design incorporates an automated mechanical ejection system (see section 10.4). In the event of an obstruction, this system will activate, creating a clear channel for water to pass. This proactive measure directly benefits downstream farmers by preventing potentially devastating floods, affecting crops, and safeguards local ecosystems by maintaining the necessary water supply for aquatic life and wetland preservation.

Furthermore, the absence of fast-moving parts and the design's low rotational speed inherently reduce the risk of mechanical injury during operation and maintenance, contributing to the overall safety of the design for operators and the surrounding environment.

Finally, leveraging the wheel's power generation capacity offers an opportunity to promote water conservation through accessible irrigation methods such as drip irrigations systems, such as the one seen in *Figure 9.3*. By powering these techniques, which deliver water directly to the desired area, this can significantly reduce water consumption in agriculture, contributing to more sustainable water resource management in the region.



Figure 9.3 – Drip irrigation system [36]

9.4 Product Disposal

Emphasising sustainable and recyclable materials from the outset ensures that the wheel's disposal phase will contribute very little to landfill. Its design for simple disassembly facilitates the separation of components for efficient recycling. Moreover, the minimal construction involved in its deployment allows for easy detachment from mooring points and removal from the canal using standard equipment. This ease of removal directly supports efficient replacement, minimising power disruption for local communities reliant on the energy generation and enabling a quick changeover to a new unit. This design also reduces long-term ecological impact by simplifying maintenance and minimising prolonged disturbances to local wildlife and ecosystems, aligning with sustainable design goals.

10 Mechanical Design

The following section outlines the mechanical design of the 1:2 scale prototype system that was built for this project, detailing the key steps taken in developing the waterwheel. This process involved careful planning, and iterative refinements to ensure optimal performance, efficiency, and durability. To streamline the design and facilitate manufacturing and assembly, the waterwheel was divided into four primary sub-assemblies:

- Channel Modifiers Used to modify the shape of the flume at the University of Southampton Science Park in Chilworth. (Figure 10.1)
- Wheel Core rotating component of the system responsible for harnessing the kinetic energy from the flowing water in the channel.
- Frame Structural support for the system to maintain rigidity, reduce flex, provide the system with buoyancy through the pontoons, and provide a foundation for other components to be attached.
- Ballasts Responsible for distributing weight evenly across the system and the primary mechanism for the ejection safety system.

Each sub-assembly was designed with three core priorities in mind; flat packing for efficient transportation, ease of maintenance, and the ability to assemble and repair the system using only common tools. These principles were essential to ensuring that the waterwheel could be widely distributed, easily deployed in various environments, and maintained with minimal technical expertise.

By designing the system to be flat-packed, we optimised it for costeffective global transport and storage with an aim to be able to fit the entire system on a single pallet. This reduces logistical challenges and makes the system more accessible to communities with limited resources. The aim of designing the waterwheel to be modular allows for quick assembly and disassembly, enabling users to transport and set up the waterwheel with minimal effort.

Furthermore, the design emphasises standard off-the-shelf components ensuring repairs can be carried out with widely available tools and materials rather than requiring specialised equipment or personnel. This enhances the long-term sustainability and practicality of the system, making it well-suited for deployment in remote or resource-limited areas.

The following sections provide an in-depth look at the design methodology, challenges, and solutions implemented for each of the before mentioned sub-assemblies.

10.1 Channel Modifiers

10.1.1 Function

The channel modifiers consist of two nearly identical walls that serve two primary functions. Firstly, since most irrigation canals feature straight vertical side profiles rather than tapered trapezoidal ones, modifications were made to the flume at Chilworth to better replicate real-life conditions and ensure more accurate testing. Secondly, the width of the channel needed to be reduced as the prototype being designed had a width of 1.5 m and the test flume at the science park had a width of 2.1 m as shown in *Figure 10.1*.

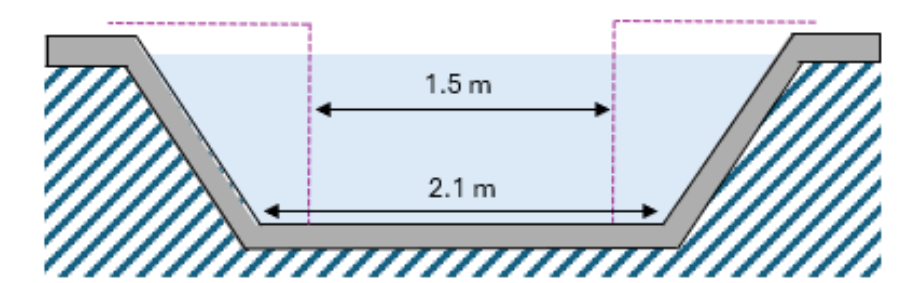


Figure 10.1 – Changes of channel width due to channel modifiers

10.1.2 Entrance and Exit Tapered Walls

A critical design consideration for the channel between modifiers was the configuration of the entrance and exit regions, which were specifically engineered to have as little impact on the flow as possible. To achieve this, the entrance length was designed to be approximately twice the width reduction, promoting a gradual contraction that minimises flow disturbances and energy losses. Although this design approach is not derived from a formal mathematical model, it is widely supported by empirical observations and hydraulic engineering practice. Literature such as Chow and USBR recommends transition lengths between two to three times the width change to prevent flow separation [37][38]. This reduction in cross-sectional area naturally increases the flow velocity within the channel, which is not a direct requirement, but was considered in the theory when calculating the initial flow velocity.

10.1.3 Manufacturing and Materials

Figure 10.2 illustrates each stage of the manufacturing process from start to finish. To ensure the modifiers could withstand water flow in the channel, a frame was constructed using T-slot aluminium extrusion and wooden fence posts (step A). This provided a solid foundation. Waterproof 9 mm PVC sheeting was then used for the panelling due to its strength and durability (step B). Plywood platforms were installed on either side of the structure (step C). Finally, the modifiers were positioned within the channel at intervals of 1.5 m, as originally planned (step D).

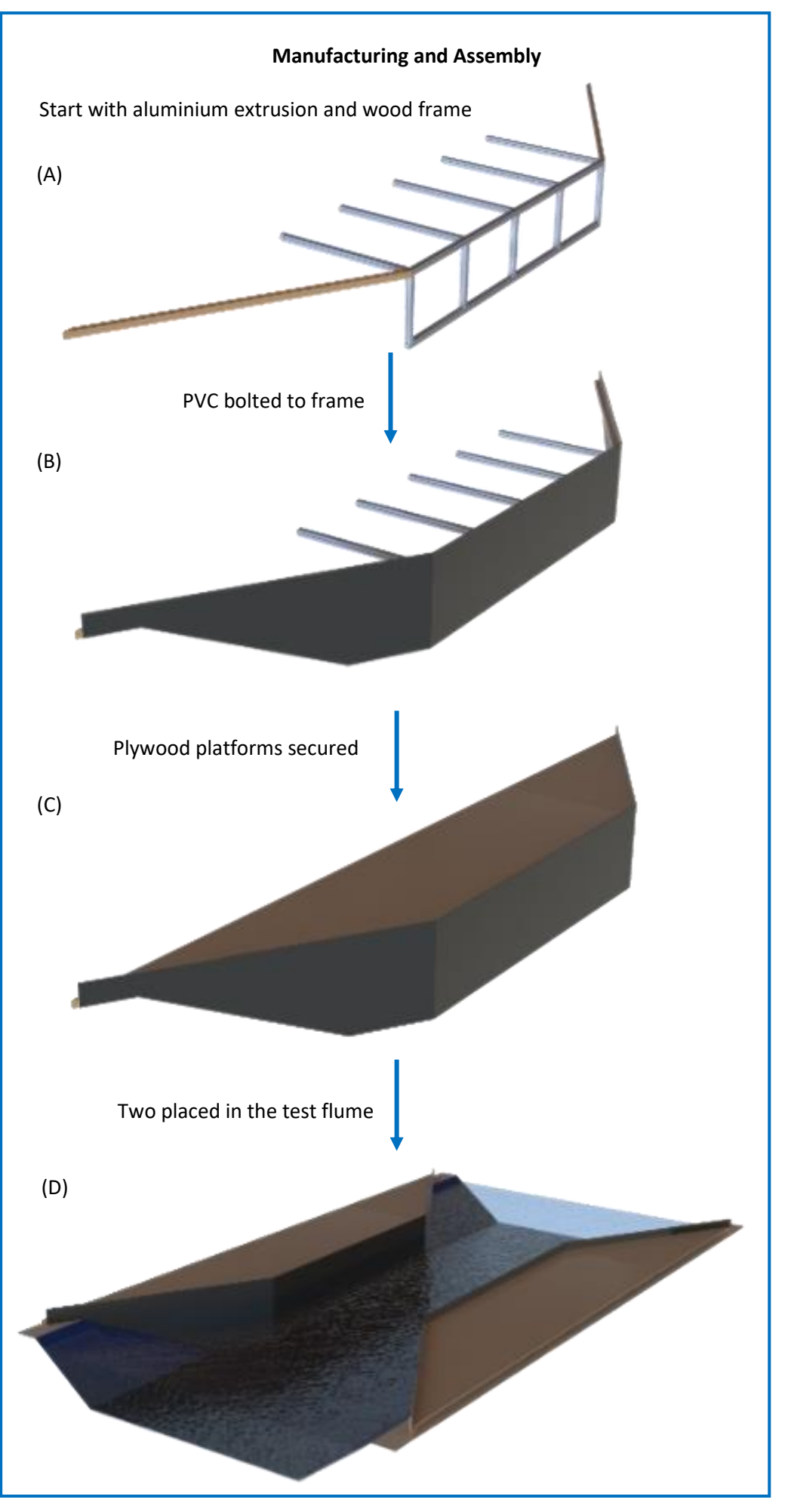


Figure 10.2 – Manufacturing stages of channel modifiers

10.2 Wheel

The wheel sub-assembly can be divided into 3 key components:

- Central Hubs
- Blades
- Shaft and Connectors

After reviewing existing literature, it was determined that the wheel's radius should be twice the submerged depth of the blades [31]. Given an initial channel depth of 0.35 m, the target submerged blade depth was set at 0.30 m. This led to the conclusion that the total wheel diameter needed to be approximately 1.2 m, immediately indicating that the wheel would be large. With this in mind and the requirement for the system to be flat-packable and easy to maintain, several design approaches were considered.

10.2.1 Central Hubs

The central hubs are essential for attaching the blades to the shaft, enabling rotation and energy generation. The initial design proposed a much larger hub with a diameter of 0.9 m and smaller blades (see *Figure 10.3*), but this proved impractical due to excessive material use and machining requirements. The blades were too short, causing water to flow over them once a head difference was created, so modifications were made to address the issue.

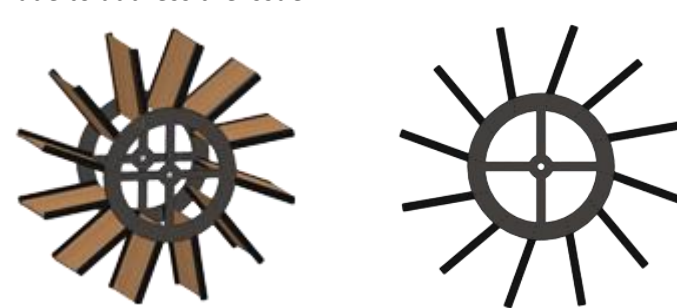
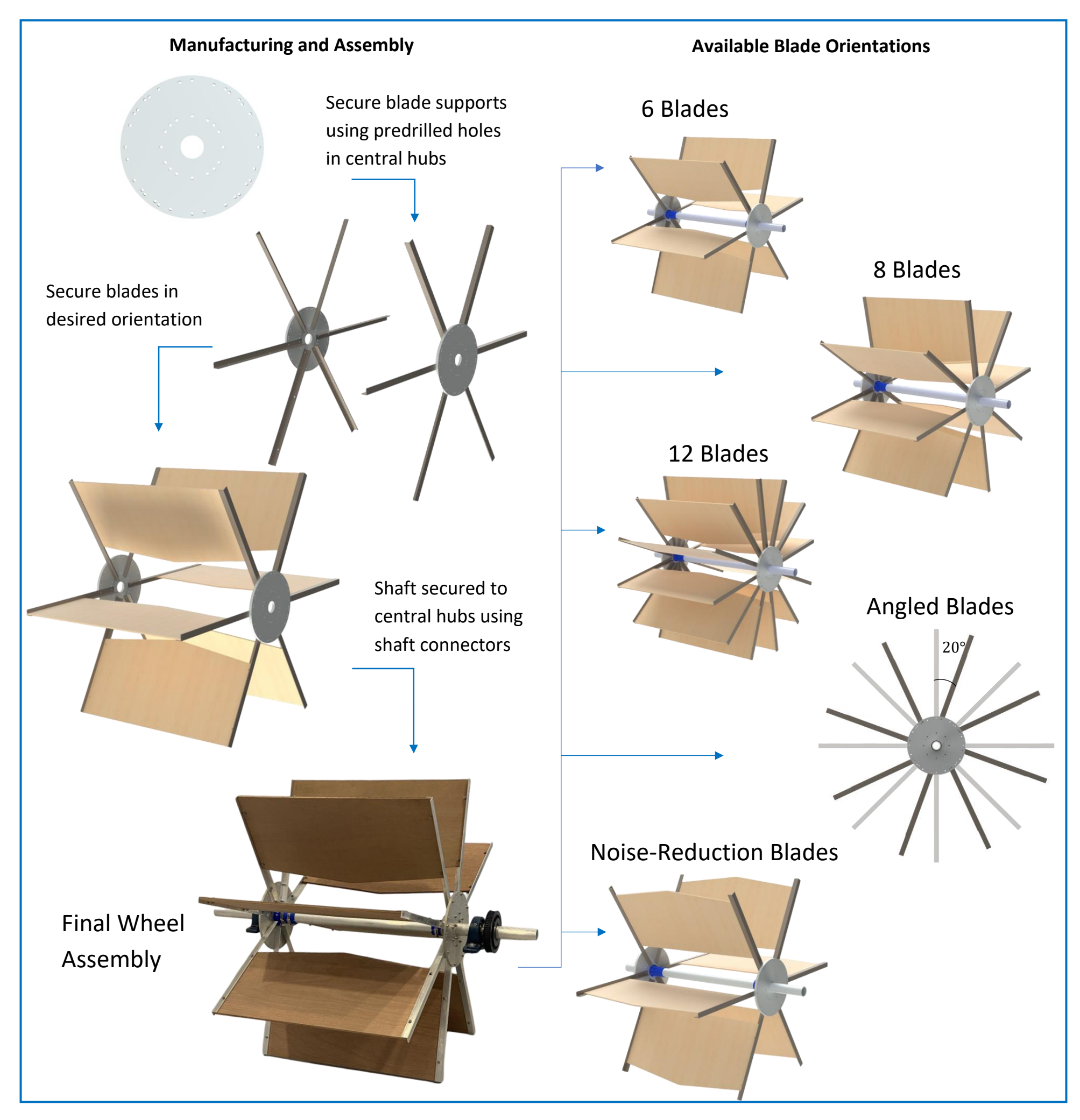


Figure 10.3 – An early design iteration to the central hubs

Instead, the solution was a compact circular design with an outside diameter of 0.3 m where the blades could be fastened simply using M6 nuts and bolts. The design features a circular hub with multiple hole spacings (top left render in *Figure 10.4*), allowing for flexible testing configurations. These holes support an alternative blade angle, 20° for potential efficiency gains and different blade counts (6, 8, or 12 shown on the right-hand side of *Figure 10.4*) to test the optimal number in terms of energy generation and power quality.

The hubs were waterjet cut from aluminium, chosen as it is lightweight, corrosion resistant, and suitable for wet environments. These hubs were one of the only components used in the design that were manufactured using specialist equipment unlike the rest of the wheel's components.



10.2.2 Blades

The optimum blade width based on theoretical analysis was between 0.6 m and 0.8 m as shown in *Figure 6.6* in section *6.3.2*. 0.8 m was used due to the fact that the pontoons had to be 0.6 m in total (see section 9.3.3) and the blades had to bridge the gap between them.

As mentioned in section 9.3, the original rectangular blade design was revised as it was apparent that flat-edged blades could generate unwanted noise on water impact. To mitigate this and consider social and environmental impacts, a tapered edge was introduced. The blades were made modular and reversible, enabling testing with both flat and tapered edges.

As shown in *Figure 10.5*, two tapering styles were explored, a curved edge and a straight-cut edge. The straight cut (*Figure 10.5*, far right) was chosen for its ease of manufacture. This noise reduction however would have a detrimental effect on power generation and efficiency. This was investigated in section 14.8.

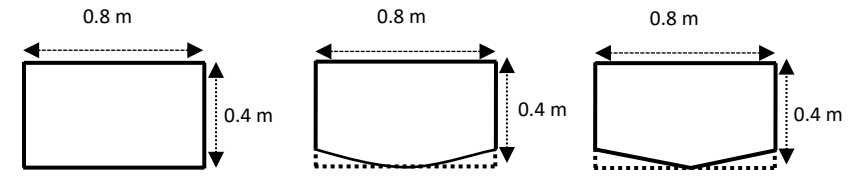


Figure 10.5 – Noise reduction blades options

The blades were attached to the central hubs using right-angled aluminium extrusion (seen in *Figure 10.4*), chosen to maintain a flat-packable and easy-to-maintain design. These extrusions are standard off-the-shelf components, making them easy and inexpensive to replace if needed. They were secured to both the marine plywood blades and the central hubs using standard M6 nuts and bolts. The holes in both the blades and aluminium bars were positioned to allow the blades to be quickly flipped 180 degrees, enabling easy testing of the tapered edge configuration. This design feature allowed for rapid experimentation and adjustment during testing, as shown in *Figure 10.6*.

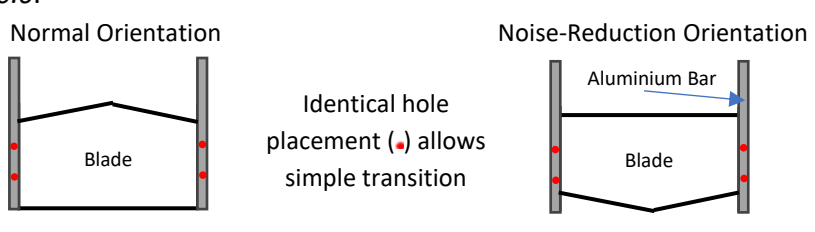


Figure 10.6 – Hole placements for reversible blades

10.2.3 Shaft and Connectors

The shaft diameter was determined by available resources at hand which included two 50 mm pillow bearings, leading to the selection of an aluminium shaft with an outside diameter driven by the bearings. Aluminium was chosen for its light weight, durability, and suitability for wet environments. It was chosen to be hollow to reduce weight and costs. The shaft was secured to the central hubs using the connectors found in *Figure 10.7* below.



Figure 10.7 – Two shaft connector iterations, blue found in final design

The shaft connectors were 3D printed using PLA plastic. The original design (black – left) used M4 nuts and bolts to clamp the connector around the shaft. However, this created stress concentrations around the bolt holes, leading to damage and insufficient strength. Additionally, the plastic-on-aluminium contact provided insufficient friction, causing the connector to slip under load. In the revised design (blue – right), jubilee clips were used instead of bolts. This change distributed the clamping force evenly around the entire cylindrical surface, reducing stress concentrations and improving both strength and friction. Furthermore, to improve the friction, a 3mm thick rubber layer was placed between the connector and the shaft. These changes resulted in a sufficiently strong component.

10.3 Frame

The frame served as the structural backbone of the entire system, providing the foundation on which all electronics, mechanical components, and supporting systems were mounted. It not only supported the wheel assembly but also contributed directly to the system's buoyancy and stability on the water by being the bridge between the wheel and the pontoons. The design focused on modularity, ease of maintenance, and the ability to be flat packed for transport. The complete frame was made up of four key elements:

- Exoskeleton
- Wooden Components
- Pontoons
- Ballasts

10.3.1 Exoskeleton

The exoskeleton of the platform was built using T-slot aluminium extrusion, selected for its modularity, strength-to-weight ratio, and ease of assembly. The overall dimensions were chosen to balance stability on the water with the need for portability and compact storage, making it ideal for flat-packing and solo maintenance. To ensure the wheel sat at the correct height relative to the waterline, support brackets were designed, also out of extrusion, and attached to the frame. A rear "backstage" section was integrated to house the powertrain (section 10.5) and provide it with a dedicated space.

Two stiffeners were included to improve structural integrity, one of which also functioned as a mounting point for the enviro-weather sensor (*Figure 10.8*). Furthermore, the entire system was moored to the side of the channel. This was done using metal cables at the front attached to two right angle brackets. Ratchet straps at the back were used for adjustability before, during and after testing to keep the system in the correct place.

The modular nature of the exoskeleton meant the entire frame could be easily assembled, disassembled, or modified, which was essential for rapid prototyping and making last minute changes when needed. This also meant that the waterwheel could be assembled by anyone using simple tools and no technical training is required. The final aluminium exoskeleton can be seen below in *Figure 10.8*.

Brackets for Mooring

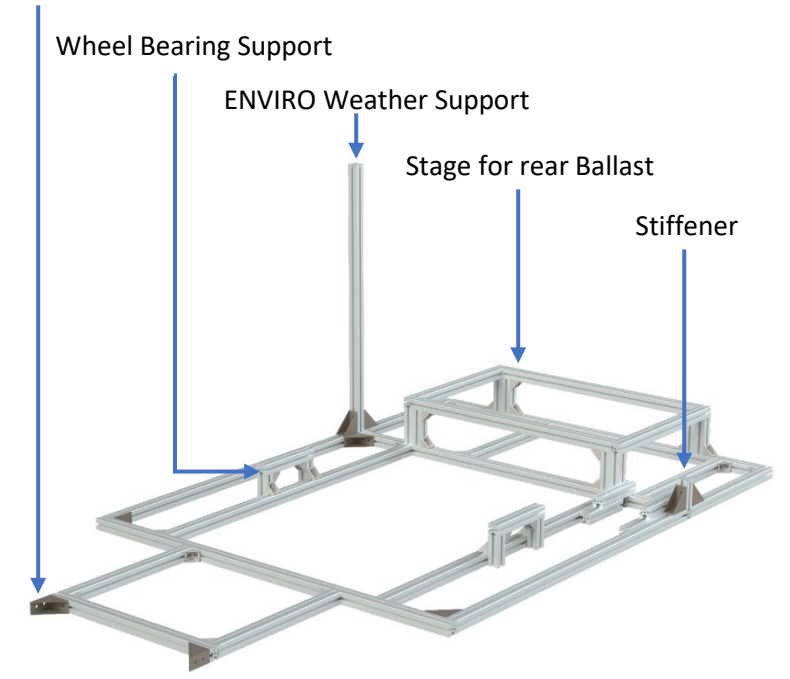


Figure 10.8 – Frame exoskeleton

10.3.2 Wooden Components

To enhance the structural rigidity of the frame, two U-shaped plywood boards shown in *Figure 10.9*, were added to the design and secured to the bottom of the frame leaving a vacant space in the middle for the wheel assembly.

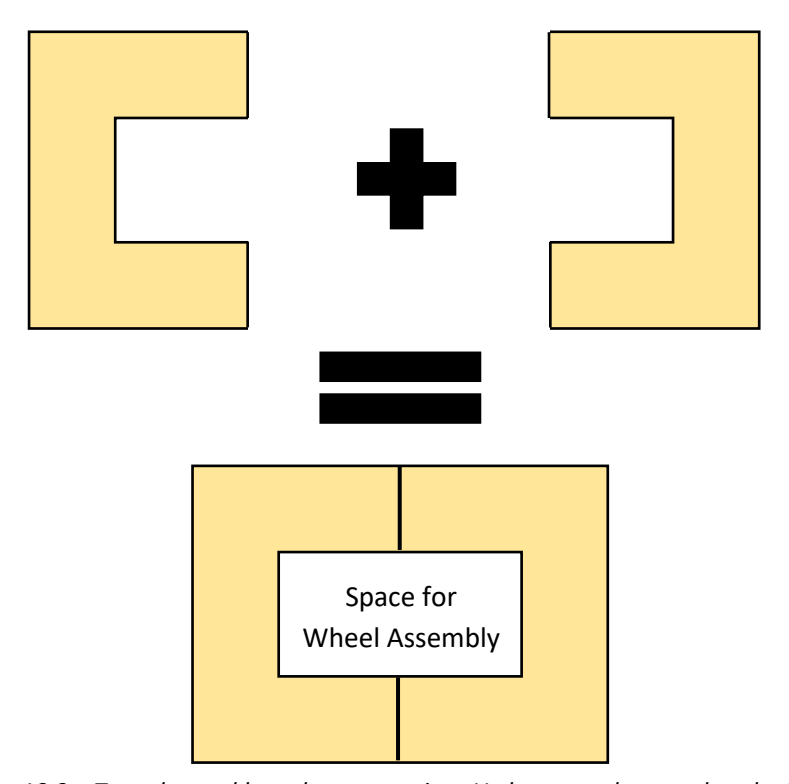


Figure 10.9 – Two plywood boards were cut into U-shapes and secured to the frame

A few materials were investigated for the frame of the system. Primarily PVC, plywood and marine plywood were looked into. However, it became apparent that if normal plywood was used, thicker sheets could be purchased (12 mm) for a fraction of the cost compared to the other two. Therefore, plywood was selected for its low cost and ease of manufacturing, making it ideal for a prototype, even if not intended for long-term use. There was also a section of plywood providing additional strength at the front of the frame to support the weight of the permanent ballast (see section 10.4). These wooden elements were mounted to the aluminium extrusion exoskeleton using off-the-shelf 90-degree aluminium brackets, creating a secure connection without adding unnecessary complexity. Beyond structural reinforcement, another rectangular section of plywood was used at the rear of the system to provide a platform where the 100- litre ballast could be positioned. This platform had to be raised above the area where the powertrain is located due to insufficient space. Like the rest of the design, these components were lightweight, flat-packable, and easy to transport, crucial qualities for the projects aims and objectives. These wooden components are shown in Figure 10.10.

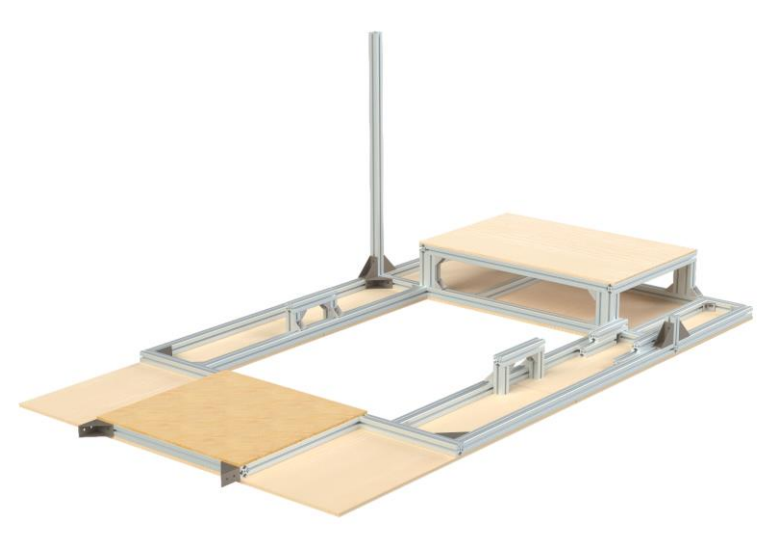


Figure 10.10 – Wooden components added to aluminium extrusion frame

10.3.3 Pontoons

The pontoons used in the design were fabricated from extruded polystyrene (XPS) foam, selected for its lightweight, buoyant, and easily machinable properties. An industrial foam-cutter was used to shape the foam into pontoons with the required dimensions. The final width of each float was influenced by economic considerations, specifically to minimise material waste and cost. The foam sheets were supplied in standard dimensions of 0.6 m width, 2.5 m length, and 0.1 m thickness. To optimise material usage, each sheet was halved lengthwise, allowing two floats to be produced from a single sheet. As a result, only four sheets were required to manufacture all eight pontoon sections, significantly reducing material expenditure. These dimensions are illustrated in *Figure 10.11* below.

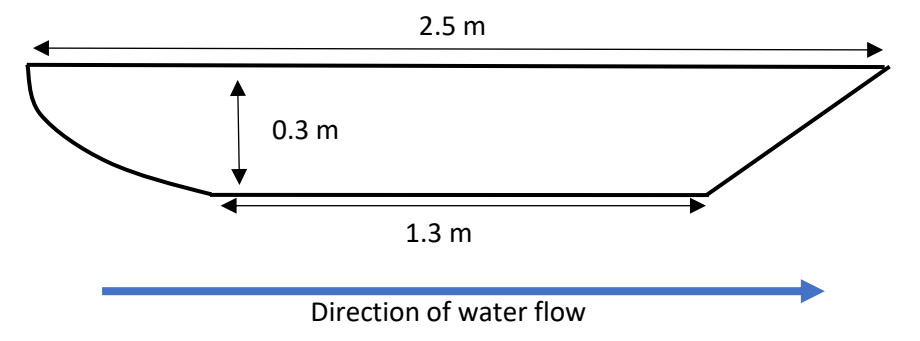


Figure 10.11 – Design and dimensions of floats – birds-eye view

The front of each float was shaped with a curved inflow profile to reduce flow disturbance and improve hydrodynamic performance. This design helps streamline water around the pontoons, minimising drag and wave generation. Such curvature is commonly used in marine applications [39], as it promotes smoother, more laminar flow compared to flat-fronted shapes, resulting in greater stability and efficiency for the system. In contrast, the rear of the pontoons featured a straight edge to allow clean flow separation at the outflow. This helps reduce wake turbulence and drag, contributing to the water flowing between the floats more efficiently.

The floats were secured to the frame using Gorilla Glue, with four layers of XPS foam bonded together to achieve the required total height of 0.4 m. Once stacked, the assembled foam was then glued to the wooden section of the frame, forming the complete the assembly shown in *Figure 10.12*.



Figure 10.12 – Pontoons and frame assembly

Before committing to the final construction, this gluing method was thoroughly tested using spare foam and wooden offcuts to verify its reliability. These preliminary trials assessed the bond strength, adhesion quality, and curing consistency under similar conditions to those expected in operation. As a result, the most effective adhesive application technique was identified, ensuring a secure and durable connection between components in the final structure.

The pontoons provided the buoyant force needed to keep the system afloat, but to achieve the desired operating depth, this had to be balanced with added weight. Water ballasts were used to counteract the buoyancy and ensure proper immersion of the system. Together with the frame and pontoon structure, these ballasts allowed for finetuning of the system's stability (discussed more in the following section). Putting all these components together, a final frame assembly is shown *Figure 10.13*.

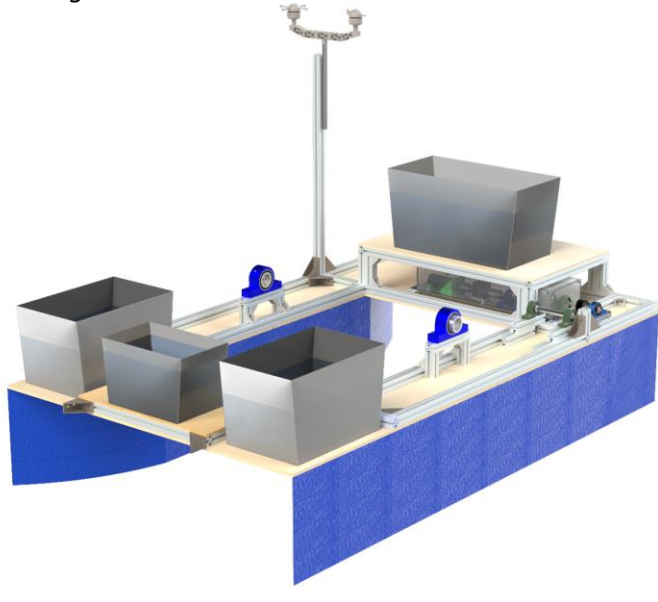


Figure 10.13 – Frame Assembly with powertrain

10.4 Ballasts / Ejection System

The ballasts located around the frame were used for two reasons:

- Provide enough weight to balance the buoyancy force of the pontoons so the system sat at the correct depth in the water.
- Act as a mechanism for ejecting the entire system out of the water in case of an emergency.

10.4.1 Buoyancy Calculations

The following table shows the key components found on the system and their respective masses given that there were 12 blades on the wheel assembly (i.e. maximum system mass).

Table 10.1 – Mass of system used for buoyancy calculations

Component or Sub-Assembly	Total Mass (kg)
Powertrain Assembly	20
Wheel Assembly	46
Aluminium Extrusion	30
Plywood	20
Foam	15
Total	131

Table 10.1 indicates that the system reaches a maximum mass of 131 kg when the wheel assembly is fitted with 12 blades. With the buoyancy force counteracting the system's weight, it was observed that, when the ballasts are empty, the system rests 11 cm deep in the water, leaving a 24 cm gap between the floats and the channel bed (as shown in the bottom image of *Figure 10.14*).

As shown in *Figure 10.14*, a 35-litre water ballast was permanently installed at the front-centre of the frame. This was kept full during testing to counterbalance the weight of the rear-mounted powertrain and maintain a level orientation.

To reach the required operational depth, the system needed to weigh approximately 350 kg, an increase of 219 kg from the initial mass. To achieve this, two 65 litre ballasts were installed at the front, along with a 100 litre ballast at the rear. Together, these provided the necessary weight for proper submersion and the balancing pitch (front two ballasts compared to rear) and roll (front two ballasts).

Emergency Ejection System Full Ballasts The plugs are pulled due to the increase in water level and the ballasts located around the frame, two at the front and one at the back, are emptied, reducing the weight of the system and causing it to rise out of the water. **Empty Ballasts** 0.24 m

Figure 10.14 – Ejection system transitioning from full ballasts to

10.4.2 Ejection System

The ability of the ejection system to raise the assembly out of the channel when needed was a critical and practical feature of the project for several reasons:

- Flood prevention in debris-heavy conditions Irrigation canals are
 often subject to the accumulation of debris such as leaves,
 branches, and waste. The ejection system allows the assembly to
 be lifted completely out of the water, preventing blockages or
 system failure, and ensuring the channel is not obstructed.
- Protection during extreme weather events The assembly can be pre-emptively raised before storms or surges, reducing the risk of damage from high water flow.
- Manual removal for maintenance and repairs In cases where automated ejection isn't feasible, the system can still be manually lifted out of the channel, allowing for quick access during routine maintenance or unexpected mechanical issues without needing to lift the entire system out of the channel.

The ejection system works using a novel design illustrated in *Figure 10.15*. As the frame rises relative to the channel wall due to a blockage, the string comes under tension. The plug is then pulled upwards allowing the water to escape and the system to rise further due to the reduction in weight.

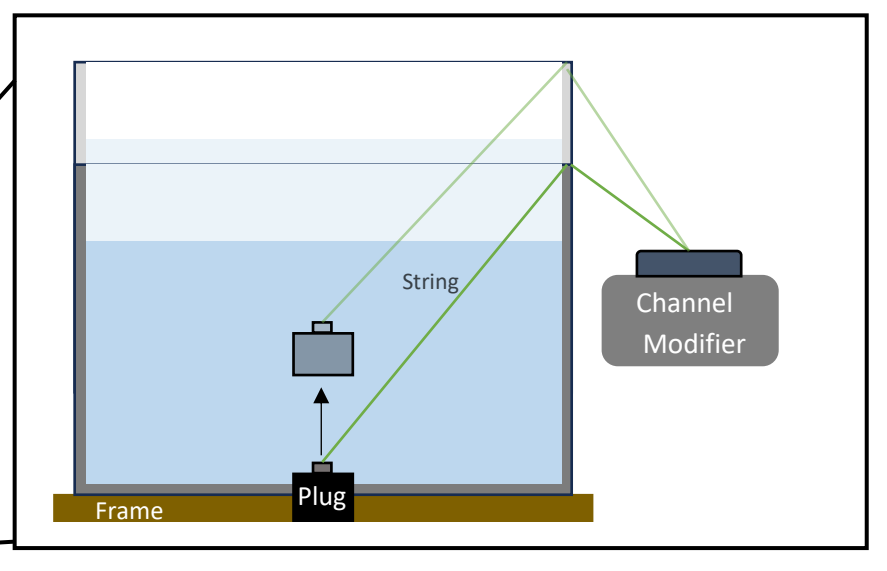


Figure 10.15 – Mechanical ejection system mechanism

Although the design required considerable fine-tuning of the string lengths, it effectively demonstrated the feasibility of the mechanism. As a proof of concept, it establishes a basis for more sophisticated developments, which are examined in greater detail in section 16.2.

10.5 Powertrain Design

To generate electrical power from the mechanical power of the wheel and to also obtain the required data, it was necessary to design a bespoke powertrain for our concept. This design also had to meet the requirements of the overall project:

- Generate electrical power from the mechanical power of the wheel
- Include a torque transducer for data collection
- Low cost to meet the overall project requirement
- Small and modular design for ease of transport and set up (meets overall project requirements)

10.5.1 Generator/Motor selection

Due to the time and cost constraints of the project, the method of electricity generation was decided to be an off the shelf DC motor driven by the wheel. The first stage of the design process was to select and purchase this motor as the required power transmission ratio would be reliant on its specification. From prior theoretical calculations for the wheel concept, requirements for the motor were drawn up:

- 1. < 60 W power rating
- 2. Low output rpm (as near to 4 RPM as possible)
- 3. Capability to be driven backwards (as a generator)
- 4. Motor type should be brushless DC

From theoretical calculations the wheel design was expected to produce around 60 W power and spin at around 4 RPM. For the DC motor to not be burnt out, it was necessary to only view motors with power ratings above this 60 W value. For maximum efficiency in power generation, this motor would have to be spun at the same rpm as its

rated output speed. To minimise the transmission ratio required between the wheel and the motor, it was also necessary to investigate motors with a rated speed as close to the expected rotation speed of the wheel.

In electric motors, rotor volume is proportional to power over speed. As a result, motors run at very high speeds for a specified power to minimise the size of the motor. Suitable motors were therefore those that already had high ratio gearboxes attached with the capability to be spun both ways.

To use the motor, it was necessary for it to be DC so it could be run using a standard power source. As the motor would also be near water, it was decided that this should be a brushless DC motor, to prevent it from being affected by water. The motor chosen can be seen in *Table 10.2* below. The max rated power of 102 W covers the fact that power could increase by 50% due to more blades being in the water as mentioned in section 6.3.2.

Table 10.2: Motor specifications

, ,		
	Supplier	Digikey
	Product manufacturer	ISL Products International
	Name	MOT-I8149-L
	Motor type	Brushless DC motor
	Gearbox type	Planetary
	Transmission ratio	77:1
	Max rated power	102W
	Rated speed	58rpm
	Rated voltage	24DC
	nated voitage	2400

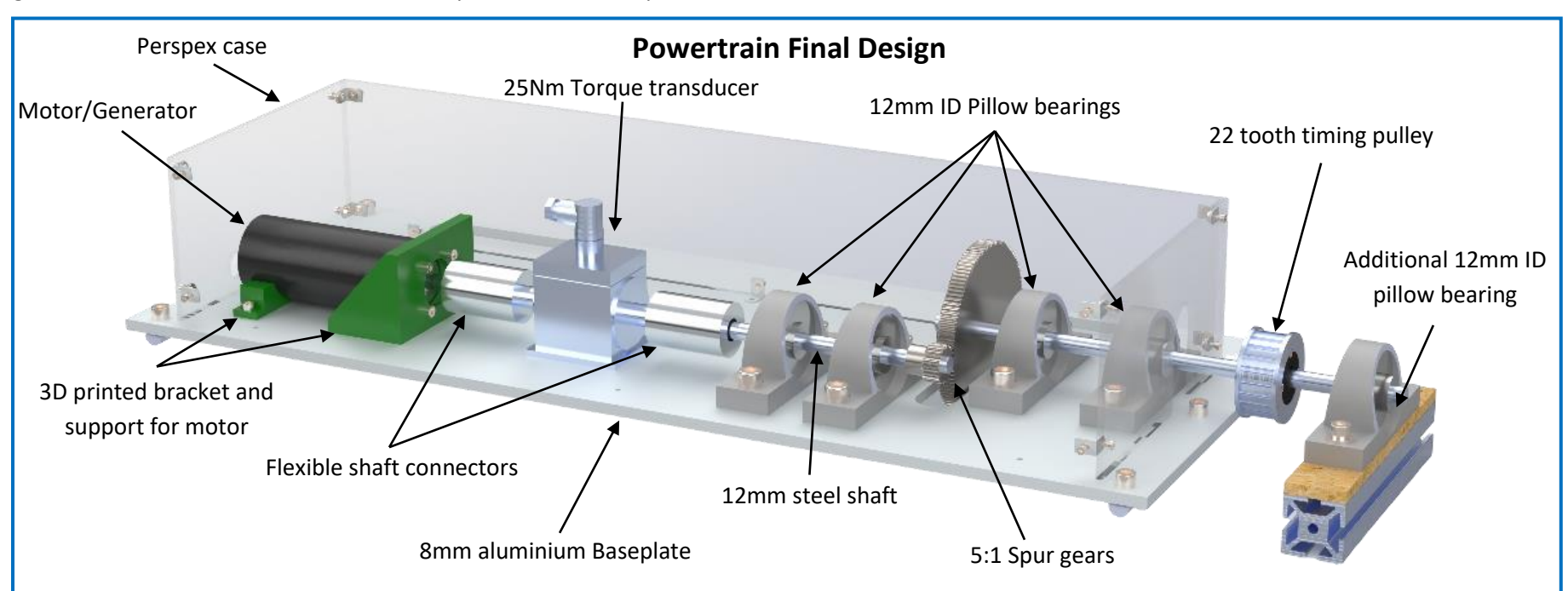


Figure 10.16 - Final powertrain design

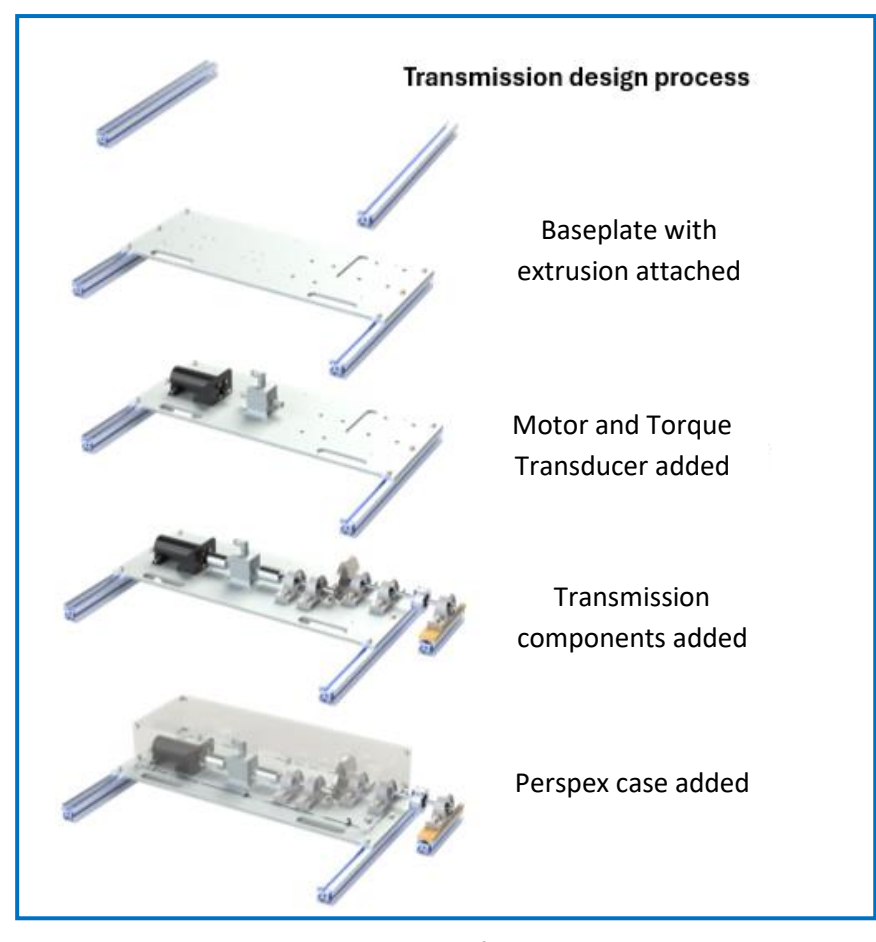


Figure 10.17 - Design process for transmission system

10.5.2 Power transmission design

After the motor had been selected, requirements for the power transmission from the wheel to the motor were drawn up.

- 1. Power transmission is such that powertrain is placed in appropriate space on the wheel
- 2. 15:1 transmission ratio (from approximately 4 RPM wheel speed to 60 RPM required motor speed)
- 3. Direction of rotation reversed from wheel to motor to balance wheel torque
- 4. Power transmission can be driven both ways

For the first requirement to be fulfilled, it was the decided that a belt drive should be used. This allowed the powertrain unit to be taken away from the wheel centre and placed behind or in front of the wheel where space was available. This placement was also helpful in terms of buoyancy and pitch as the powertrain mass could now be balanced out by the ballast tanks.

A few concepts using just belt drives were considered, however the required transmission ratio meant that either the ratio of pulley diameters would be unfeasible, or the amount of belt drives and pulleys required would make the system too complex. To add to the complexity, to meet requirement three with just belt drives, a cross-belt drive system would have to be employed.

As a result, the final design was decided to be a mixture of two transmission solutions, a 3:1 belt drive that took the power away from the centre of the wheel to the back, followed by a 5:1 spur gear set-up that not only would take the speed up to the required RPM but would also meet requirement three by reversing the direction of rotation.

10.5.3 Final design

The final design can be seen in *Figure 10.16*. The main powertrain unit sits on an aluminium waterjet cut base plate of dimensions 770×300 mm. This module can be attached and detached easily from the wheel making it ideal for flat packing.

The module sits on two 40 x 40 mm aluminium extrusions attached to the wheel frame and is fixed by three M8 bolts and T-nuts either side. The module can easily be slid back and forth along these extrusions by hand using the handholds cut in the base plate, to pretension the belt coming from the wheel shaft.

To attach both pulleys, the 150 mm diameter pulley to the wheel shaft and the 50 mm diameter pulley to the 12 mm steel shaft of the main powertrain module, two taper locks were used. To prevent the pulleys from slipping, two pins were manufactured. These were placed through holes drilled into the shafts and slotted into the keyway of the taper lock as shown in *Figure 10.18*.

Similarly, to prevent the gears and the shaft connectors from slipping during use, sections of the 12 mm steel shaft were filed flat. This was done to aid the grub screws gripping to the shaft (*Figure 10.19*).

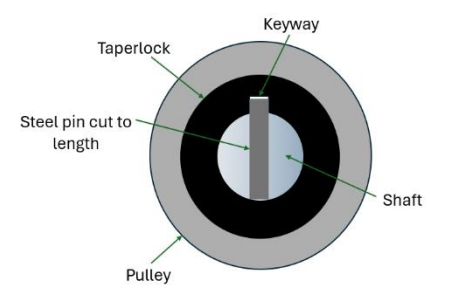


Figure 10.18: Pulley to shaft attachment method

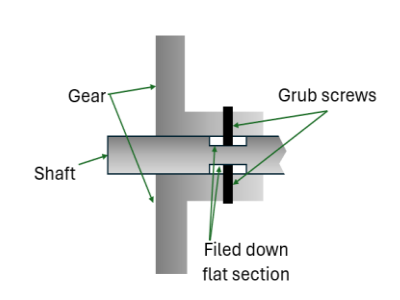


Figure 10.19: Gear to shaft attachment method

Originally, the belt drive and pulley system used was a V-belt. However, after testing this system by spinning the wheel by hand, it was discovered that even after tensioning, the V-belt did not have the required friction to overcome the resistance of the generator (motor in reverse). The belt and pulley system were therefore changed to a timing belt with a similar ratio of 2.9:1 resulting in a transmission ratio of 14.5:1. The teeth of the timing belt allowed for increased friction

with the pulley, meaning the belt could now overcome the resistance of the motor without slipping.

Although the belt could be pretensioned by sliding the baseplate along the extrusion, further tensioning was required afterwards to again ensure the belt did not slip. This was done using another 12 mm steel rod placed through two more 12 mm ID pillow bearings placed along the bottom of the belt. The set-up can be seen in the *Figure 10.20* below.

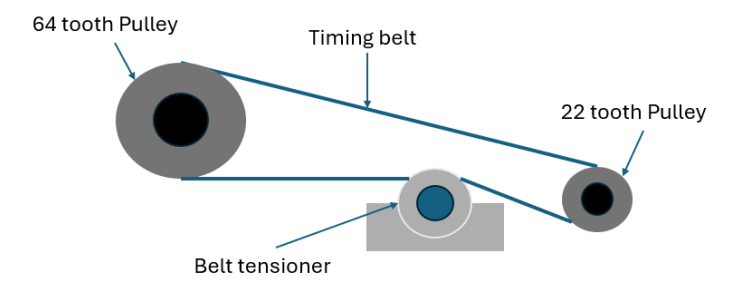


Figure 10.20: Schematic diagram of belt drive and tensioner

10.5.4 System Losses

The output power measured at the generator will be lower than the theoretical maximum power calculated from the head difference and the flow velocity due to several losses. These losses can be categorised into three areas as shown in the Sankey diagram below (*Figure 10.21*).

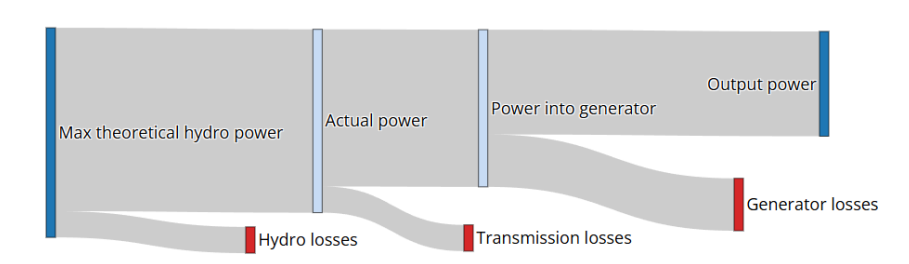


Figure 10.21: Sankey diagram showcasing losses in wheel system

To calculate the efficiency of our design, it is necessary to quantify the magnitude of these losses. The three loss areas are characterised by the following mechanisms.

Hydrokinetic

- Impact losses will occur when the water hits the wheel blades
- Leakage between the wheel blades and the channel walls and bottom
- Boundary layer separation at the channel modifiers will cause turbulence in the flow giving less potential energy for the wheel to exploit

Transmission

• Power will be lost in the transmission from the wheel to the generator due to the friction of the rotating parts.

 Power will also be lost through slippage and flexing of the belt drive

Generator

- Resistance in the copper windings of the generator will cause a power loss proportional to the square of the current produced
- Armature losses within the permanent magnet of the motor due to hysteresis effect and induced eddy currents
- Mechanical losses within the generator due to the friction of the rotor and the air resistance to the rotor (windage)

10.5.5 Test/Measurement plan

Generator losses

The simplest of these losses to measure are those exhibited by the generator. By measuring the input torque, T_{in} into the generator, the speed of the wheel, ω_{wheel} and using the transmission ratio to convert to the speed into the generator, the input power, P_{in} , of the generator can easily be calculated using the formula:

$$P_{in} = T_{in} \times 14.5\omega_{wheel} \tag{10.1}$$

The generator losses, P_{gen} , can then simply be calculated by taking the difference between the measured output power of the generator, P_{out} , and the calculated input power, P_{in} .

$$P_{gen} = P_{in} - P_{out} (10.2)$$

Generator losses results are discussed in section 14.5.

Transmission losses

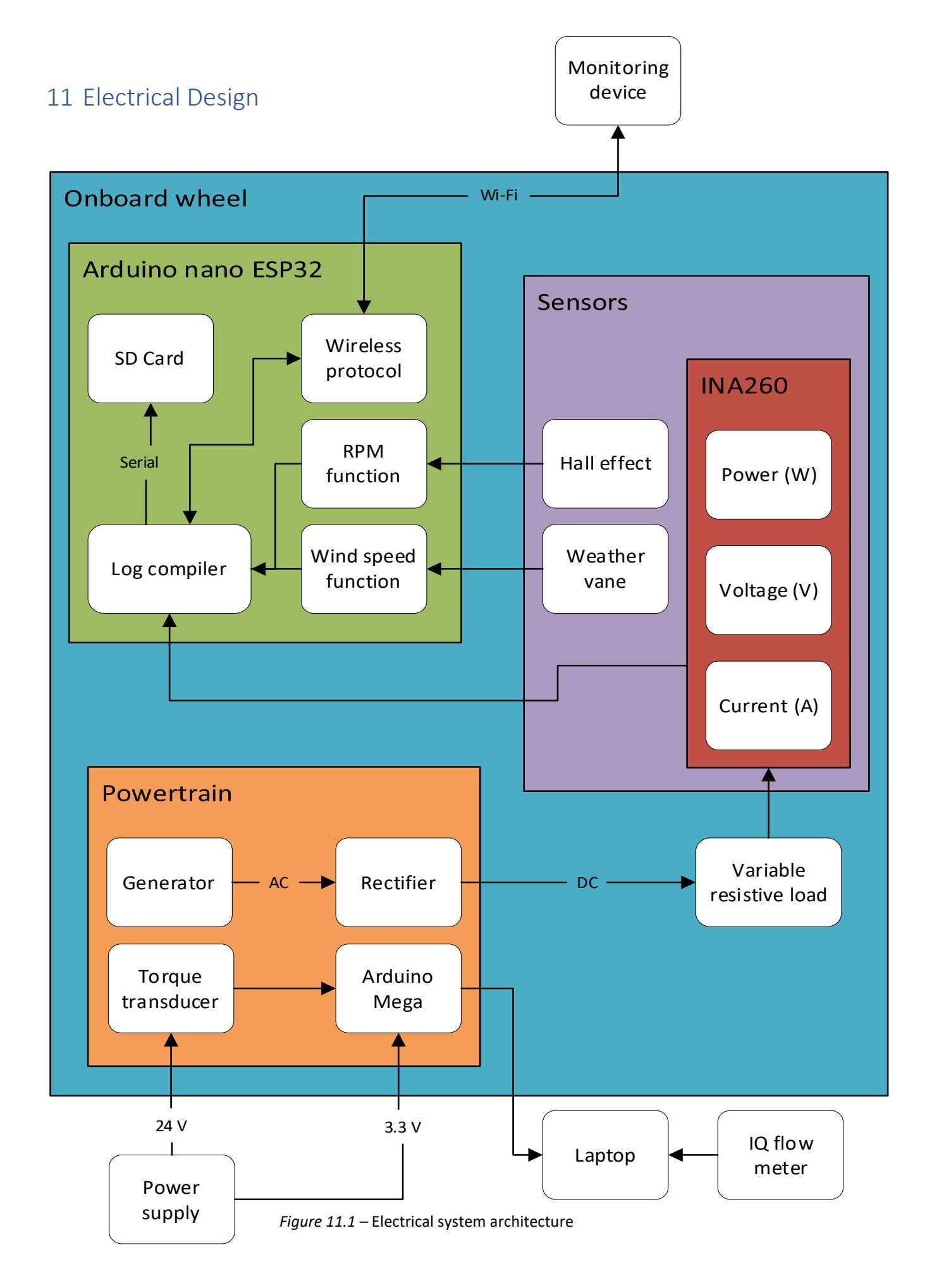
By reversing the direction of drive and turning the wheel with the generator as a motor while outside of the water, the transmission losses can be measured. This is done by measuring the output torque of the motor, T_{out} , required to overcome the friction of the transmission and drive the wheel at a set constant speed, ω_{wheel} . Again, using the transmission ratio to convert to the speed of the motor, the power required to overcome the frictional resistance in the power transmission, P_{mech} , can be calculated.

$$P_{mech} = T_{out} \times 14.5\omega_{wheel} \tag{10.3}$$

The mechanical power loss, P_{mech} , will vary for different wheel speeds. However, as the torque required to overcome the friction of the transmission, T_{out} will remain constant, once measured, it is simple to calculate P_{mech} for a range of different wheel speeds. The results from the transmission losses test are discussed in section 14.1.

Hydrokinetic losses

It is challenging to measure the losses caused by the impact of the water on the blades and the boundary layer separation at the channel modifiers. As a result, the hydrokinetic losses will not be considered in any analysis.



11.1 System Architecture

Designing the electronic system for the wheel comprised of three main aspects, the power-take off from the motor, sensors for assessing wheel performance and subsequent data handling. The systems intended for future wheel design all fed into one central Arduino that handled data processing and output. Systems purely dedicated to performance assessment were connected to a separate external laptop. The overall design architecture of the system can be seen in *Figure 11.1*.

For the central Arduino an ESP-32 Nano was selected, a decision driven primarily by its integrated Wi-Fi and Bluetooth capabilities. Additionally, the ESP-32 offers superior processing power and memory compared to other Arduinos, such as the traditional Nano. These enhanced capabilities as well as the compact size compared to other microcontrollers with similar computing capabilities meant that the ESP-32 Nano was deemed the most suitable option for the project.

11.2 Data Handling

Following the selection of the ESP-32 Nano as the central processing unit, a key element of the data handling strategy involved the implementation of a wireless live plotting system as well as a local data logging system.

11.2.1 Wireless and live plotting

During testing, sensor data was monitored in real-time using a wireless system built around the Arduino microcontroller. The Arduino acted as a password-protected Wi-Fi access point, allowing client devices (e.g., laptops, phones) to connect. Users accessed a web interface via the IP address '192.168.4.1' in a browser, establishing a WebSocket connection. Upon connection, the client device transmitted its current timestamp to the Arduino, ensuring all subsequent data logs were accurately time-referenced. This automated timestamping eliminated manual synchronisation efforts and potential errors during post-processing. The browser interface displayed live metrics such as power, RPM, current, and wind speed without requiring custom software.

For more advanced live analysis and data logging, a Python script was created to connect to the same WebSocket stream. This script continuously stored the data and provided live plots displaying the average value of metrics over a user-configurable time window (default 30 seconds). This allowed operators to easily record averaged performance data, smoothing out instantaneous fluctuations (like power oscillations), while also enabling the observation of longer-term operational stability by adjusting the viewing window (see example in Appendix A).

11.2.2 Data Recording

To store data recorded during testing a micro-SD card module was used. The decision was made to use this to store data locally instead of over WIFI, so that if there were any connection issues, no data would be lost. Data, formatted as JSON, was appended to a .txt file. This approach was selected for its faster write performance compared to other file handling methods on the SD card module, which struggled with frequent file open/close cycles. To optimise this further, data was buffered in groups of ten before being written to the .txt file. To reduce transmission file size and optimise storage utility, the final system will log data in CSV format.

11.3 Sensors

11.3.1 Hall Effect Sensor

RPM is a key parameter in performance analysis. A hall effect sensor, detecting magnetic field passage, was chosen over reed switches and reflective optical sensors for its non-contact nature, minimal wear, and reduced environmental sensitivity.

The sensor was mounted near the wheel's hub using 3D-printed fixings, with magnets attached via 3D-printed clips. To allow for more frequent RPM updates and faster detection of changes at the wheel's low operating speed, the initial design of a single magnet was revised to incorporate four magnets. The sensor detects magnetic field changes as the wheel rotates, sending a signal to the Arduino to calculate RPM. These RPM values were averaged to balance responsiveness and stability. The sensor mounted on the wheel is illustrated in *Figure 11.2*.



Figure 11.2 - Hall effect sensor mounted on the wheel

11.3.2 Voltage, current and Power Sensing

An Adafruit INA260 was used for sensing voltage, current and power. The sensor is able to simultaneously measure both current and voltage, providing the benefit of only needing to use one sensor. An internal 2 $\mu\Omega$ shunt resistor allows for voltage measuring of up to 36 V and a current of up to 15 A. This falls within the range our generator will be providing when operating under load. The sensor communicates with the Arduino using I2C interface, providing precise measurements up to a resolution of 1.5 mA.

11.3.3 Weathervane

Weather conditions were measured using an Enviro Weather station. An anemometer and wind vane that used reed switches to calculate the wind speed and direction were used. These were connected with an RJ11 connector to a dedicated breakout board, which then fed the information to the Arduino. Based on the reed switch activation rate on

the anemometer, the wind speed could be calculated using custom built functions. Wind direction was done using the same techniques. This kit was included as a temporary precaution so that if testing had to be conducted in poor weather conditions that might have affected test results, for example high winds, data would be available to quantify the effects this had on the performance of the wheel.

11.3.4 IQ Flow meter

To measure flow properties in the channel, an IQ Flow meter was used. This device uses five acoustic beams in combination with a pressure sensor to profile water velocity in three dimensions as well as providing depth measurements. The sensor was placed in the centre of the canal bed, upstream of the wheel, and connected via a cable to a laptop situated alongside the channel. Proprietary software was used for data acquisition and processing. Velocity data collected was used to verify flume conditions for every test as well as inform theory-based calculations to help predict total power available and produce efficiency numbers. The IQ flow meter was included in the prototype test setup but would not be needed for commercial installations of the product.

11.4 Power Take-off

11.4.1 Three Phase-Full Wave Rectifier

The brushless DC motor generated three-phase AC power, necessitating rectification to DC for compatibility with the Arduino's DC voltage sensor. A three-phase full wave diode rectifier was built to do this. The circuit diagram for the rectifier can be seen below in *Figure 11.3*. The six-diode, three-phase full-wave bridge rectifier converts the generator's AC output to DC. The inherent nature of three-phase power, where one phase is always conducting, yields a DC voltage with substantially lower ripple than that of single-phase rectifiers, producing a more stable DC signal. A smoothing capacitor is included in the circuit to further reduce output voltage ripple.

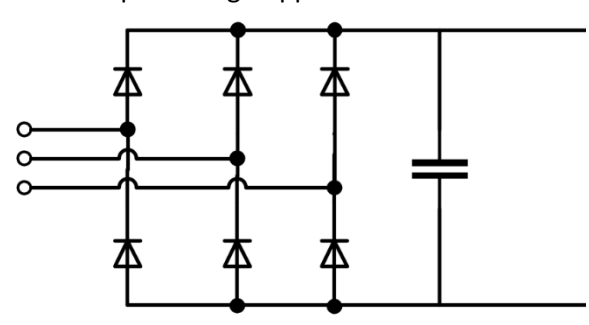


Figure 11.3 – Rectifier circuit diagram

11.4.2 Torque Transducer

As mentioned in section 10.5, a 25 Nm RT2A Torque Transducer was included in the powertrain setup, allowing the mechanical torque

produced by the wheel to be measured before being converted into electrical power by the generator. The transducer was powered by an external power supply operating at 24 V. The outputted voltages that corresponded with applied torques at a sample frequency of 50 Hz. These signals were then processed by an external Arduino Due, provided by a previous project, which transmitted data to Excel via Data Streamer for live monitoring on an external laptop. Prior to testing, the transducer outputs were validated by hanging a known weight at a known distance from the transducer and verifying torque readings were accurate.

11.4.3 Variable resistive load

To vary the RPM of the wheel, the load over the generator had to be increased. As a result, the generator requires more force to turn. This leads to more force being needed to turn the wheel, decreasing the RPM of the wheel connected to the generator. The load was varied by using resistors to control the current produced by the generator. Reducing the resistance across the generators output allows more current to flow. This increased current increases the electromagnetic opposition inside the generator, making it harder to turn [40].

Initially, variable resistors were planned for easy load adjustment. However, cost limitations prevented the acquisition of units capable of handling the high-power levels generated. Instead, a switchboard was created using normal power resistors that were rated up to 50 W. The circuit diagram for this can be seen below in *Figure 11.4*.

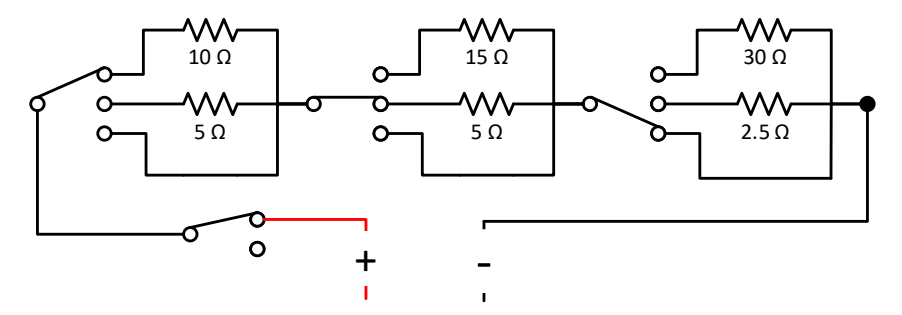
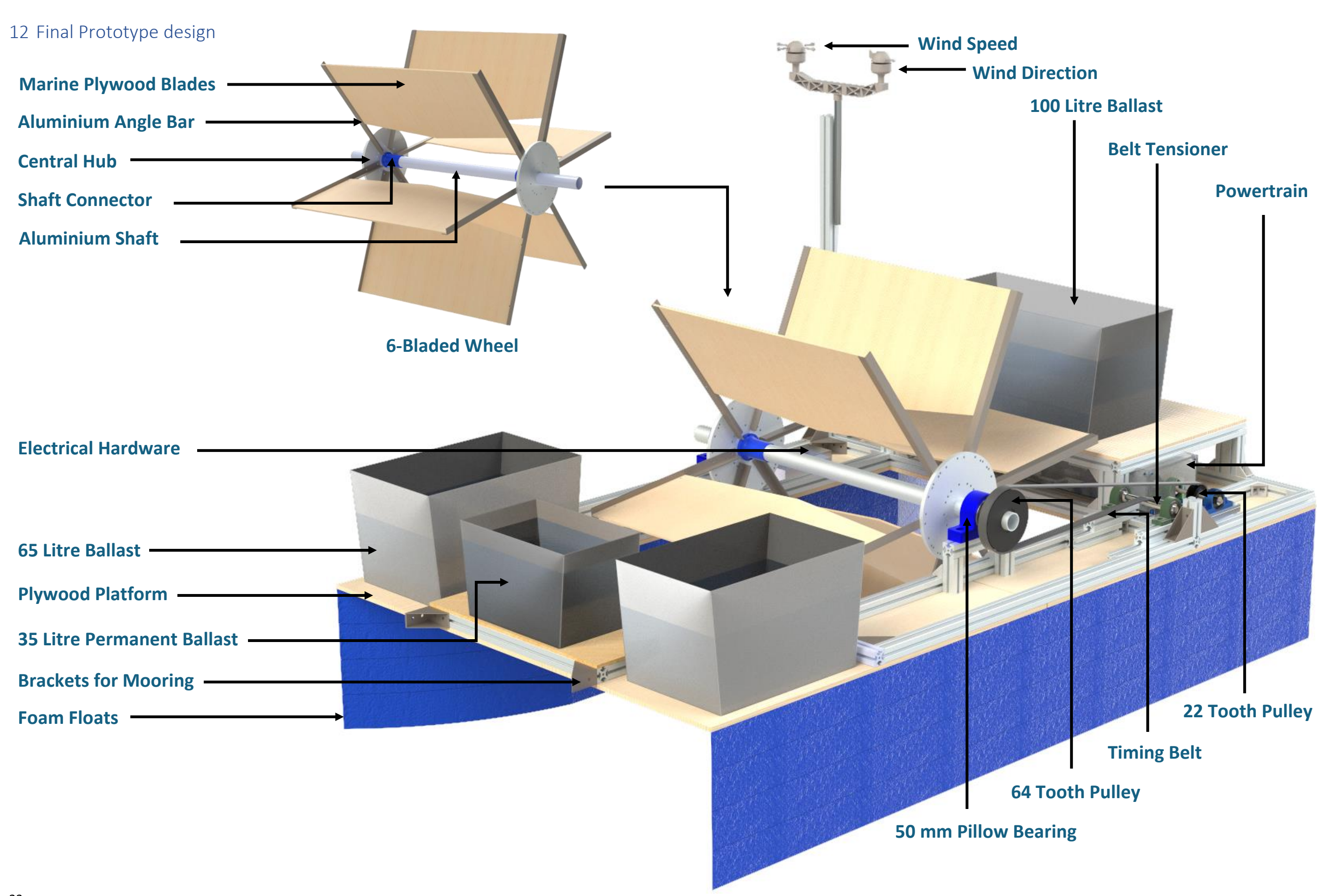
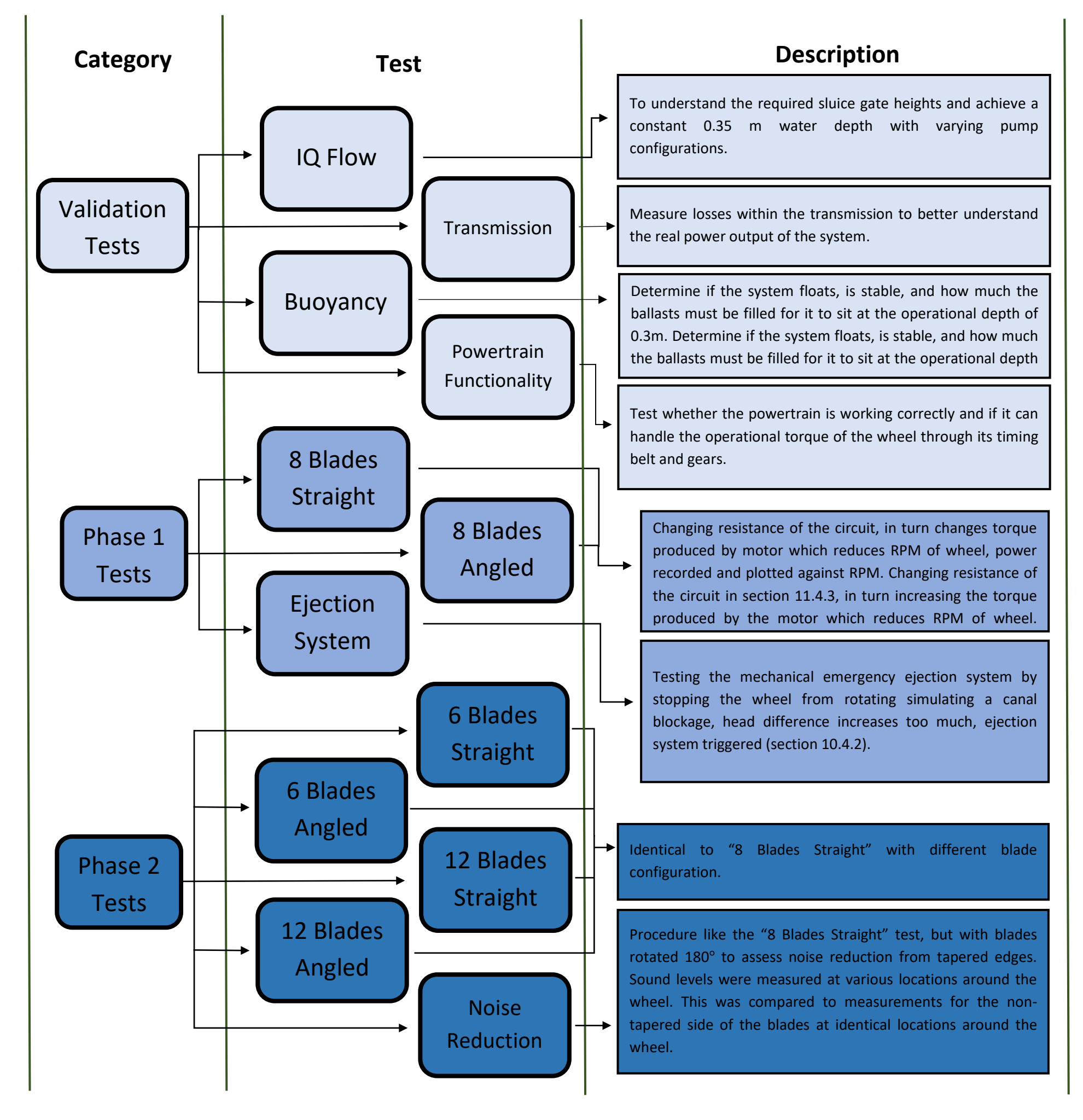


Figure 11.4 – Circuit diagram of resistor switchboard

The switchboard utilised three-way switches to enable a high degree of customisation in the applied load. This customisation was achieved by incorporating bypass wires, which allowed the resistance to be varied from 55 Ω to 30 Ω in 5 Ω steps, followed by finer 2.5 Ω steps from 30 Ω down to 0 Ω . An on/off switch was incorporated at the start of the circuit, allowing us to break the circuit at any point, essentially providing infinite resistance to the generator. This feature was incorporated into the design as a safety precaution for both test operators and the wheel. In the event of a testing malfunction, it would allow for immediate load removal from the wheel.





13 Test Plan

Before any testing began, a structured plan was developed and divided into three distinct phases to streamline the process and ensure all objectives were met:

- Validation Tests These were preliminary assessments essential to verify system readiness and inform design decisions. They included operational checks required for the use of the test facility (e.g., the IQ flow test) as well as tests that could influence design modifications. For instance, the powertrain functionality test revealed the need for improved belt tension, leading to the replacement of the V-belt with a timing belt. In summary, these tests confirmed whether the initial design met critical requirements.
- Phase 1 Tests These were the core tests required to meet the project's primary aims and objectives. This phase also served as a fallback measure, ensuring that, if subsequent components failed, the project could still be considered a success based on these results.
- Phase 2 Tests These were additional, non-essential tests intended to provide further insight into system performance. While not critical for project success, they improved the understanding of the systems behaviour. An example includes reversing the blades to their tapered edge to assess noise levels, an exploratory step aimed at evaluating social and environmental impacts.

Validation and Phase 1 tests were considered essential, while Phase 2 tests were supplementary. Thanks to an efficient and disciplined testing schedule, all planned tests, including the additional Phase 2 assessments, were successfully completed and analysed.

13.1 Method

To ensure that each test was conducted in a consistent, reliable, and valid manner, a rigid and systematic methodology was established. Central to this approach was the development of Standard Operating Procedures (SOPs) for every individual test. These SOPs served as formal, detailed documents outlining the exact steps required to carry out each test. SOPs included comprehensive step-by-step instructions, clearly defined parameters, and structured result tables to be filled out during testing. They significantly enhanced the repeatability and reproducibility of the tests. By following the same procedure each time, the likelihood of human error or test variation was greatly reduced, allowing results to be compared reliably across multiple test runs or be understood by potentially absent individuals.

An example of one such SOP is provided in Appendix B, which outlines the procedure for the IQ Flow test.

14 Results

Following the successful completion of all tests, a comprehensive results analysis was conducted to evaluate the wheel's performance characteristics. The subsequent sections detail the analysis of how varying blade number, angle, and type influence power output.

14.1 Mechanical losses in the powertrain

The test to quantify the transmission losses was carried out as described in section 10.5.6. Output torque from the motor was collected by the transducer for a set constant wheel speed of 4 RPM. The average torque was calculated as 0.56 Nm. For a wheel speed of 4 RPM, the motor must spin at 14.5 x 4 = 58 RPM. Translating this speed to angular velocity and using the equation defined in the system losses section above, the power lost due to the transmission for a wheel speed of 4rpm can be calculated

$$P_{lost} = T_{out}\omega_{motor} = 0.56 \frac{58 \times 2\pi}{60} = 3.4 W$$
 (14.1)

As discussed in section 10.5.6, this measured average torque value, T_{out} = 0.56 Nm, required to overcome the friction of the transmission can be applied to different wheel speeds to get the power lost in the transmission for that wheel speed. It is worth noting that these losses would be relatively large on the prototype compared to the final 3 m system.

14.2 Optimal blade number study

Procedure for all power tests comprised of taking varying power readings at set RPMs. Load variations on the generator were achieved by adjusting the resistance in the circuit which led to changes in the RPM of the wheel. At each RPM, the system was given time to settle before power readings taken which were then averaged over 30 seconds and recorded by the testing team. In addition, all test results were logged continuously onto an SD card at a frequency of 5 Hz. During data analysis second degree polynomials were fitted to all the data.

A study was conducted to determine the best number of blades for power generation. Identical testing was carried out on each wheel setup, varying the RPM of our wheel over a range to find the optimum. Results have been plotted in *Figure 14.1*.

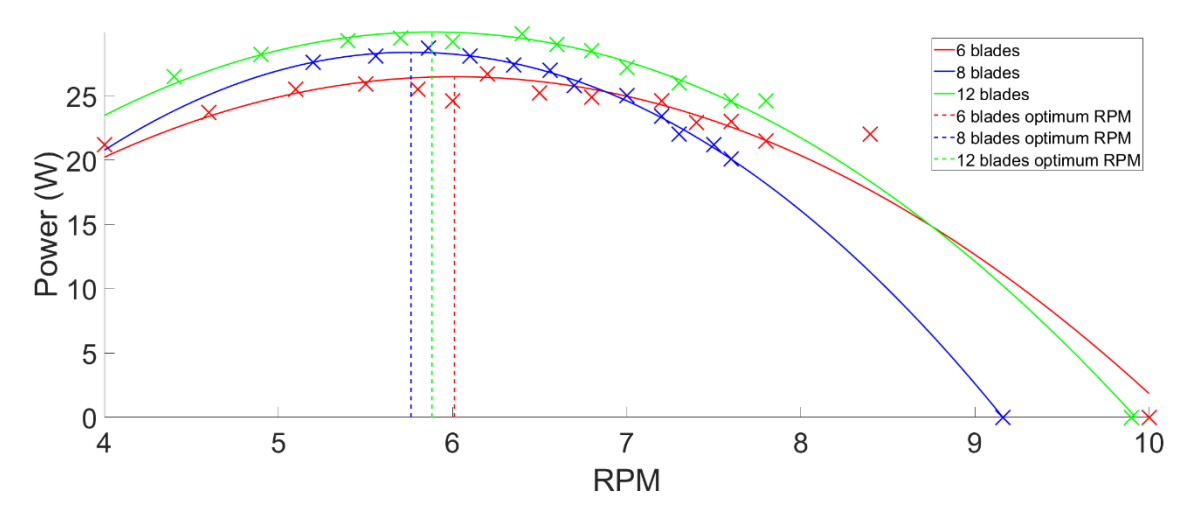


Figure 14.1 – Power vs RPM for blade number comparison study

As seen in *Figure 14.1* the best performing number of blades was 12, which when fitted with a second-degree polynomial achieved a peak power of 29.96 W, compared to 28.38 W for the 8 blades and 26.48 W for the 6

blades. Peak RPM for the 12 blades was 5.88 RPM, with the 8-blade peak at 5.76 RPM and the 6 blade at 6.01 RPM. This testing revealed a 5.57% power improvement with the 12-blade configuration over the 8-blade design. Critically, the 12-blade option requires 1.5 times more blade material. This increased material cost versus a relatively small performance enhancement should be considered when moving from a prototype to final product, as customers with specific power needs might prioritise the cost savings offered by the 8-blade configuration.

14.3 Straight Blades vs Angled for optimum blade number

Following on from the number of blades study, similar tests were carried out to determine the effect of angling blades at 20°. The theory was that angling the blades would increase the power generated. Results from the tests can be seen in *Figure 14.2* for the 12-blade setup. Due to the additional angle of the blades, if angled blades were to be as equally submerged as the straight blades, then angled blades should have been slightly longer. However, there was not the available resources to make an extra 12 blades so instead a correction factor was applied in post processing to account for the loss in blade depth. This amended data is plotted in the figure in purple.

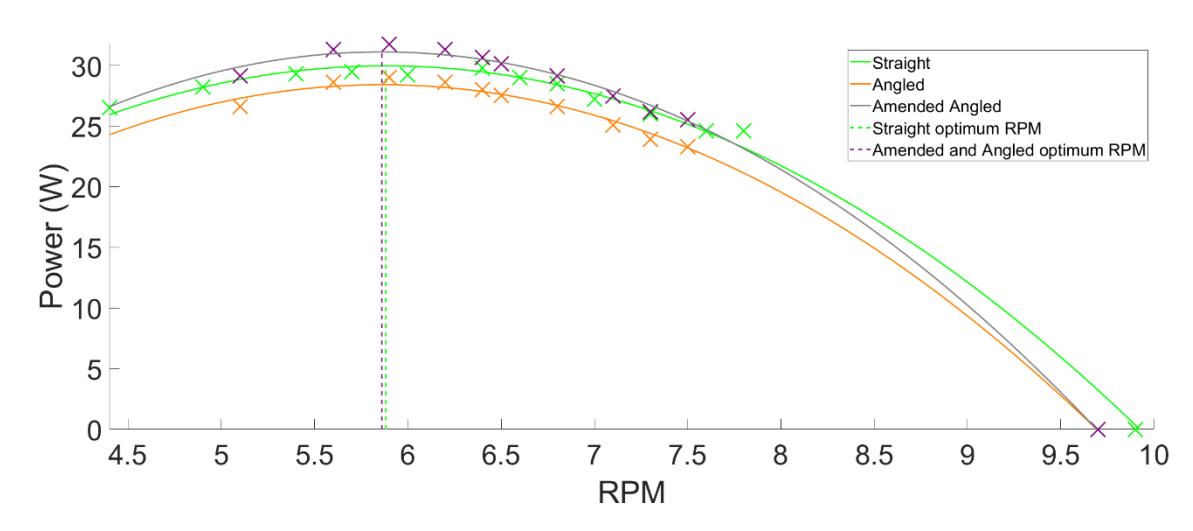


Figure 14.2 – Power vs RPM for 12 blade angle study

Results from the tests show that once the correction factor had been applied to the angled blades, the power generation was greater for the angled blades than the straight blades. The peak power was 31.6 W at an RPM of 5.69 whereas for the straight blade it was 29.96 W at an RPM of 5.88. This is a 5.47% increase in power generation when the angled blades can be assumed to be operating at the same depth. It was also observed during testing that the angled blades created more noise than the straight blades when entering the water. It was decided during the test of the angled blades that the modifications made to reduce noise generation would be tested on the angled configuration as these appeared to require the most dampening.

14.4 Power Quality Graphs

It was also observed from the experimental results that power quality varied depending on the blade configuration. *Figure 14.3* shows the raw data from the torque transducer. As the data was originally noisy, it was smoothed using a ten-point moving average. The original data can be seen faded in the figures background. The 12-blade configuration demonstrated markedly more consistent torque output than the 6-blade system, as expected. Contrary to initial expectations that the 6-blade setup might achieve higher peak torques due to reduced inter-blade flow interference, both configurations exhibited similar peak torque values. This finding is

significant, as it indicates that the increased number of blades in the 12-blade system does not diminish the maximum instantaneous torque achieved. As anticipated, the difference between peak and trough values for the 12-blade configuration were less than that of the 6-blade system, at approximately half. The combination of comparable peak torque and significantly reduced torque variation in the 12-blade setup resulted in a more consistent and higher average torque input, leading to its superior power extraction performance.

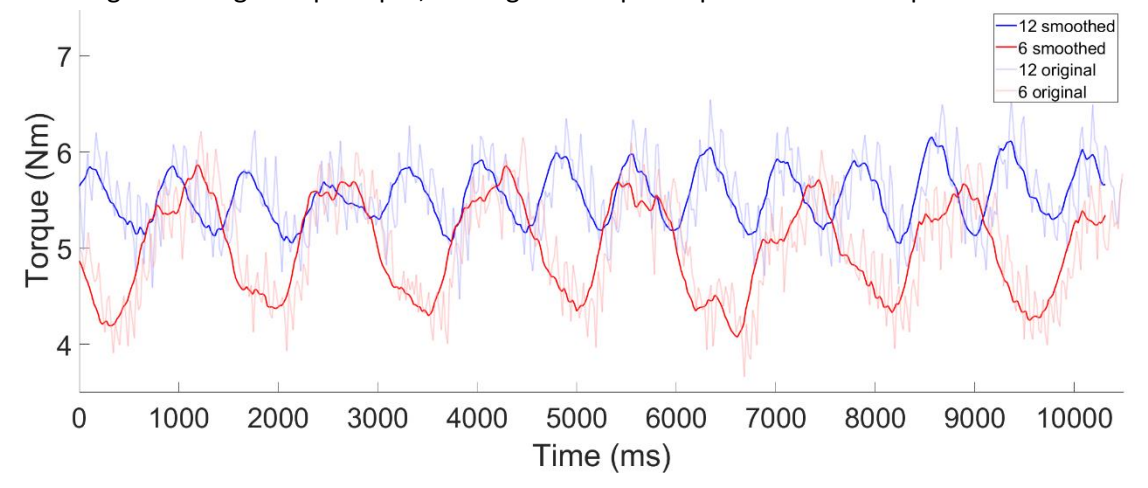


Figure 14.3 – Torque output over time for 12 blade and 6 blade wheels

14.5 Generator Efficiency

By incorporating the torque transducer into the powertrain, mechanical power going into the generator could be calculated. This allowed for the efficiency of the generator to be reported. The mechanical power compared to the electrical power generated can be seen in *Figure 14.4* below. This comparison was done for the amended angled data as this was the setup that produced the most power.

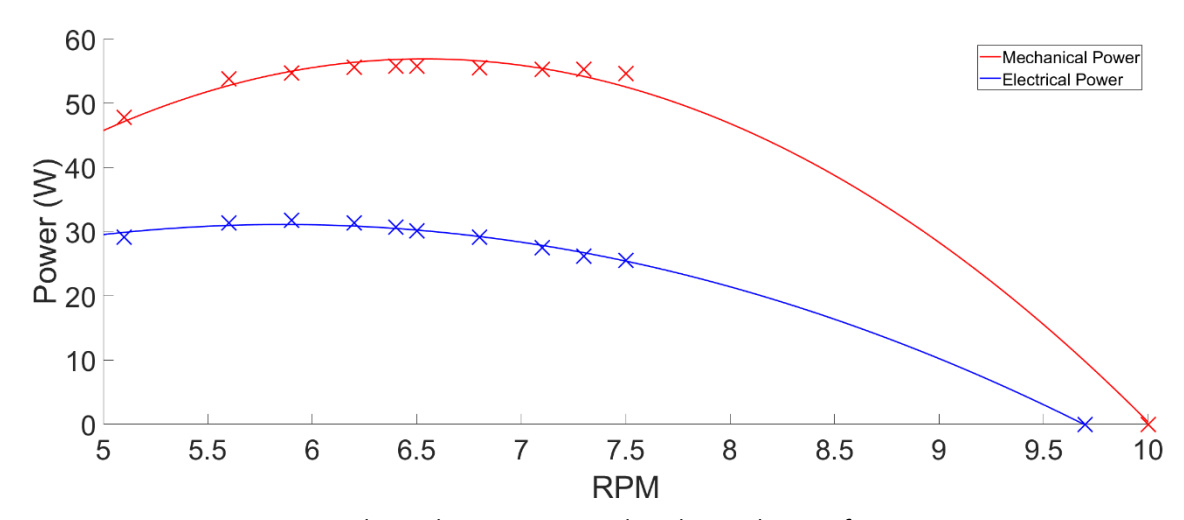


Figure 14.4 – Mechanical power compared to electrical power for varying RPMs

Figure 14.4 shows that a maximum mechanical power of 56.9 W can be extracted from the wheel, which occurs at a wheel speed of 6.54 RPM. The mechanical power depreciates significantly once the wheel speed passes 8 RPM. A maximum power of just 31.6 W was observed from the electrical power of the wheel, giving an efficiency of just 52.4%. This maximum was observed at a lower RPM compared to the maximum mechanical power, at 5.69 RPM. The low efficiency shows that there are major losses in the generator being used, with a poor conversion rate from mechanical power into electrical power as predicted in section 10.5.4.

14.6 Mechanical Power Extraction

By adding the transmission losses to the power generated at 6.54 RPM, the full mechanical power extracted from the flow can be calculated. At this RPM, the angular velocity at the generator is 9.86 rad/s and the torque is the same as above in section 14.1. This means losses are assumed to be 5.5 W, giving a maximum extracted mechanical power of 62.4 W. This can be compared to the hydrokinetic power available in the flow through the channel modifiers.

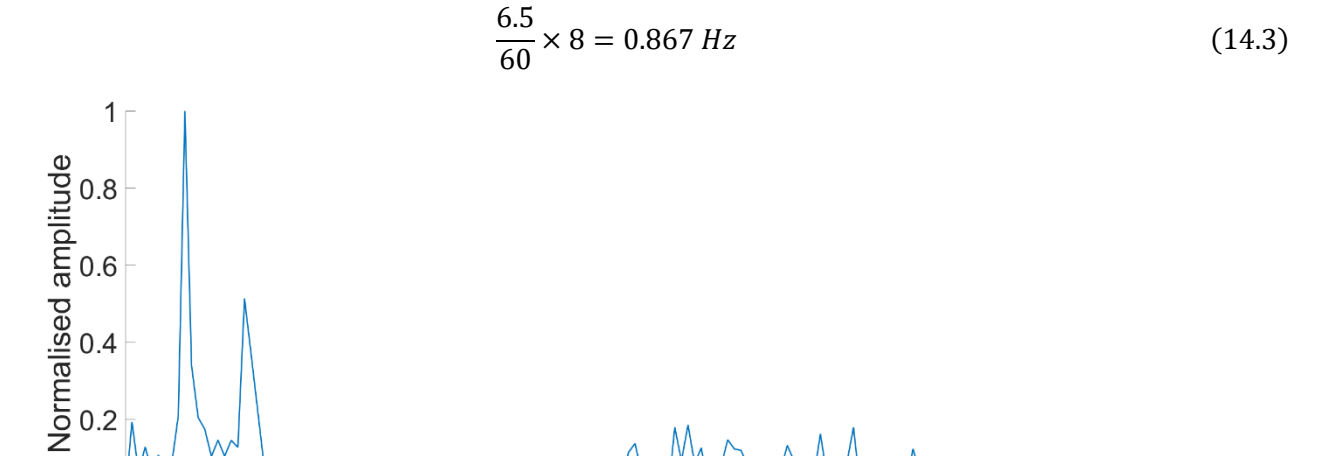
$$P = \frac{1}{2}\rho Q v^2 = \frac{1}{2}\rho A v^3 = \frac{1}{2}(1000)(0.575)(0.398)^3 = 18 W$$
 (14.2)

By creating a head difference in the flow, a 247% increase in power extraction was achieved. Power extracted can also be compared to the original theory calculations completed in section 6.3.2. The predicted power output was 59.2 W, giving an efficiency of 105%. This can appear confusing at first, however the predicted theoretical power only accounted for one blade in the water. As mentioned, (section 6.3.2) there is research to suggest that having multiple blades in the water can increase power generation by up to 50%. However, this is a maximum and an increase of 40% was used. If this is assumed to be the case, then maximum theoretical power would be 88.8 W. This would give a new approximate efficiency of 70%. This number does contain assumptions, so further research where only one blade is in the water should be carried out to verify this further.

14.7 Frequency Analysis

A Fast Fourier Transform (FFT) is a signal processing tool used to decompose a time-domain signal into its constituent frequencies. This technique was applied to the collected torque transducer data to identify the dominant frequency components, providing insight into the periodic behaviours and fluctuations in the data. The FFT was applied to a section of the data where the wheel was operating at a constant RPM, so its periodic properties were stable. The constant RPM chosen for analysis was 6.5 and the wheel configuration the data was taken from was an 8-blade setup.

Figure 14.5 shows the results of the FFT, normalised against the maximum output. Using the RPM of the wheel and the number of blades the expected blade passing frequency can be predicted.



8

Frequency (Hz)

Figure 14.5 – FFT results for 8 blade wheel at 6.5 RPM

5

6

As can be seen in *Figure 14.5*, the first peak is located at 0.855 Hz which is assumed to be the blade passing frequency. The next peak seen occurs at 1.71 Hz which is two times the blade passing frequency. This second harmonic frequency can be attributed to some misalignment in the powertrain, causing this to appear in the FFT. From this, conclusions can be made that additional losses are present in the powertrain when the system is running under load.

A more detailed study and investigation would need to be conducted to quantify the total effects this has on power generation. Following this, optimisation of the power train design would be needed to reduce this harmonic peak and increase the powertrain efficiency. As the FFT returned no other major peaks, it can be assumed that the fluctuations in the torque transducer readings are due to the reasons explained above as well as small amounts of noise. The above analysis was also carried out on data from the 6 and 12 blade configurations and returned the same results.

14.8 Audio Comparison

The three aims of the audio comparison test were to first verify that the blades modifications made a difference to the noise generated by the wheel, then to see the effect these blades had on power generation and finally try and quantify the difference in sound pressure levels at a known distance. The tests were carried out on angled blades.

Following the replacement of the standard blades, it was quickly apparent that there was a clear change in the noise generated by the wheel. The noise previously associated with the blades was unanimously perceived by the testing team to be significantly diminished with the modified configuration. The difference was particularly pronounced when standing upstream of the wheel.

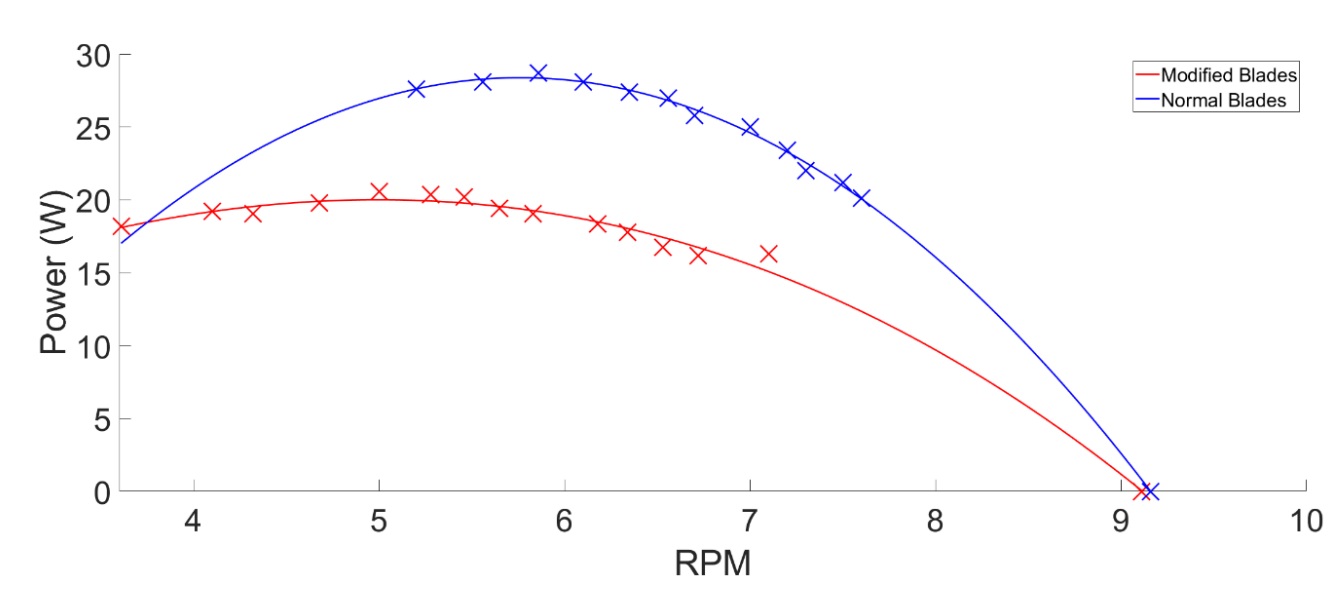


Figure 14.6 – Power against RPM for the modified blades

Figure 14.6 shows the power curve for the modified blades. Testing was carried out in the exact same manner as all previous power tests, with 8 blades. As seen, there is a significant drop in power when compared to the normal blades seen in the figure above (blue line). A surface area reduction of 12.5% led to a maximum power generation drop of 29.5%. To counteract this, more work must be done on the design of future blades, optimising them to keep maximum surface area while ensuring edges are curved enough to reduce noise.

Whilst testing the power generated by the wheel, the sound pressure level was recorded 3 m upstream using a mobile phone as a sound level meter. The hope was to compare the two recordings made by the phones and be

able to visually compare the periodic peaks seen as the blade hit the water. Raw data from the noise testing can be seen in *Figure 14.7*.

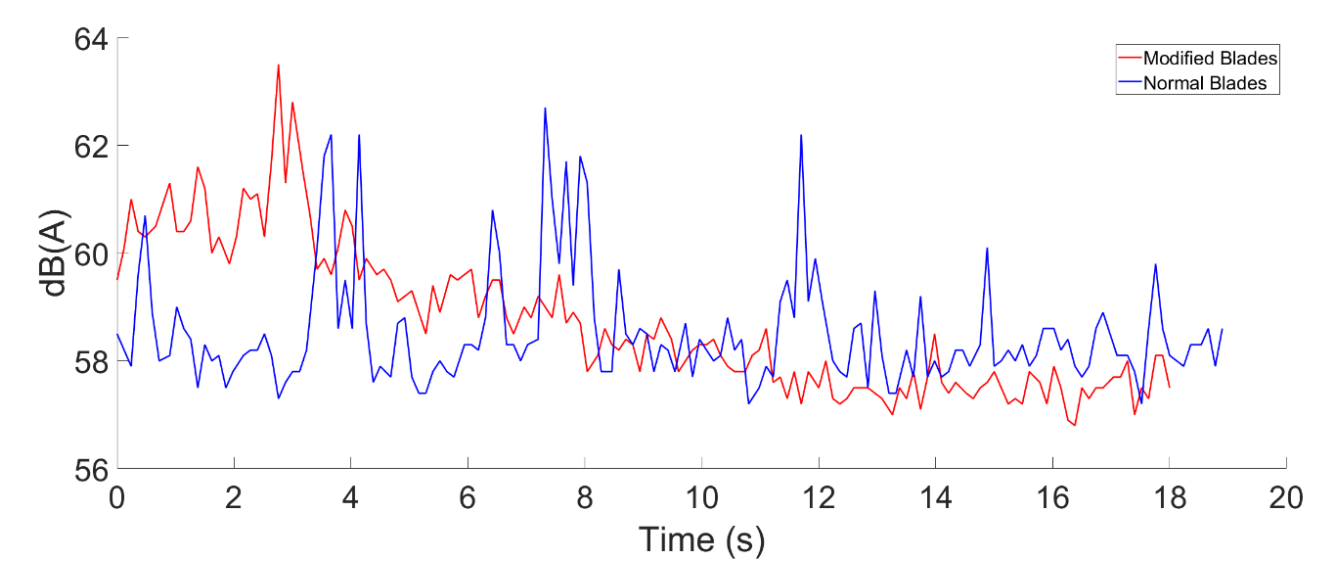


Figure 14.7 – dB(A) levels over time captured at 3 m from wheel

Visually identifying these peaks was not possible due to the quality of equipment being used and an environment with a high level of ambient noise, however the data collected was put through an FFT to see if the blade passing frequency could at least be observed.

Results were plotted for both blade types and for the testing of the normal blade edges, the blade passing frequency could be observed, seen as the major peak in *Figure 14.8 (A)*. However, this peak could not be found in the results that were captured when the modified blades were attached to the wheel in *Figure 14.8 (B)*. As test conditions can be assumed to be identical, given there were no changes to the noise environment between the two tests, this can be considered evidence that the blade modifications did make a measurable difference to the sound generation. To quantify these effects, further testing under controlled conditions with calibrated equipment will be necessary.

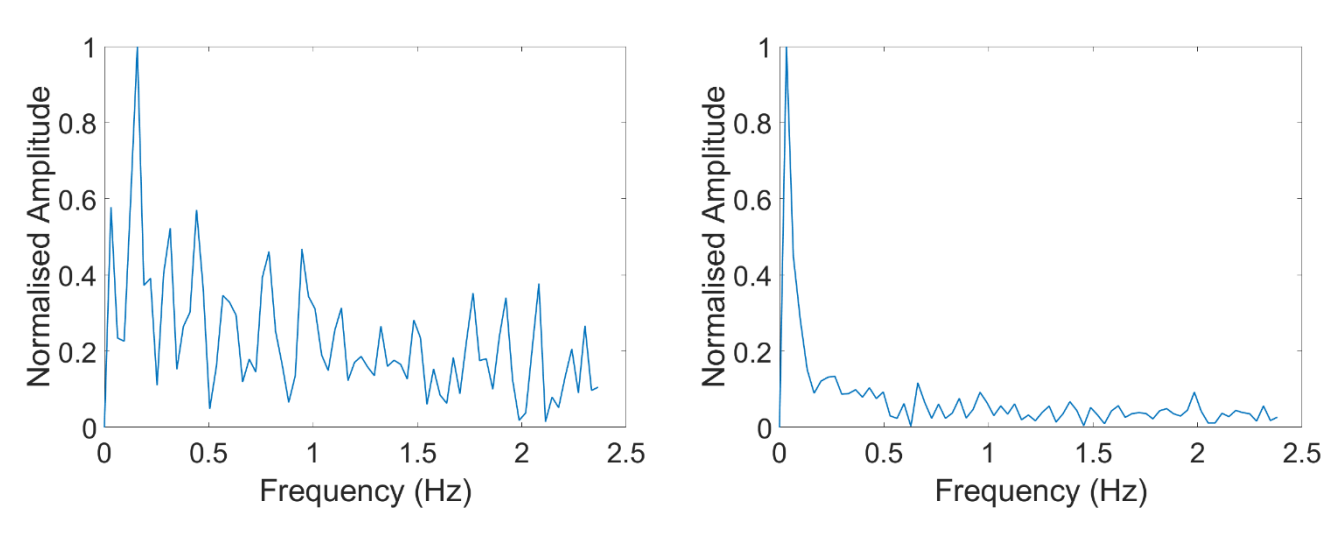


Figure 14.8 – FFT of the straight blades noise data (left - A) FFT of the modified blades noise data (right - B)

15 Critical review

The project's success was underpinned by the team's effective application of a diverse range of engineering and project delivery skills. A key outcome was the delivery of a fully operational kinetic waterwheel prototype, which successfully facilitated the testing of eight distinct blade configurations. The considerable scale of the project, with the final prototype measuring 2.8 m x 2 m x 1.4 m, also necessitated significant logistical competency.

In terms of technological maturation, evaluated using the Technology Readiness Level (TRL) scale (ranging from 1 to 9) [40], the project demonstrated substantial progress. It advanced from an initial TRL of 2 at inception to a TRL of 6 by its conclusion, indicating a significant development from basic principles to a prototype demonstrated in a relevant environment.

15.1 Innovation

The flexibility of the open brief enabled the development of several novel design solutions aimed at meeting the project's objectives, with a strong emphasis on cost-efficiency, ease of assembly, and operational adaptability.

15.1.1 Cost-Effective Manufacturing and Logistics

Innovation in this area focused on material selection and component design. The predominant use of sheet materials and simple extrusions facilitated a design that can be flat packed, significantly reducing distribution costs. Furthermore, an inexpensive, widely available geared brushless DC motor was innovatively repurposed as a generator and paired with a custom rectifier circuitry, to achieve low-cost electricity generation. Custom parts, such as shaft couplings and sensor mounts, were efficiently produced using 3D printing.

15.1.2 Novel Operational Design

The floating platform concept is a central innovation. Unlike conventional hydro systems like dams or weirs that require significant site modifications, this design generates a head difference by floating deep in the water, anchored only by mooring lines. This allows for minimal site impact and rapid deployment or removal.

15.1.3 Safety and Adaptability

The project proved the concept of an automated ballast ejection system. This novel feature allows the wheel to automatically release ballast water in response to a critical rise in canal water levels. During testing, the front plugs were pulled automatically and the ballast released. The resulting change in pitch prevented the rear ballast plug from releasing due to increased submersion. The rear plug eventually had to be released manually. The overall ejection failed to meet the

sub 3-minute requirement. Despite the suboptimal performance, the wheel rose, reducing its immersion and minimising obstruction to the canal's natural flow.

15.2 Process

The project followed an adapted double diamond process (detailed in section 4). It commenced with the establishment of a detailed specification, informed by the intended application in Spanish irrigation canals (as defined by the University of Granada) and the operational characteristics of the outdoor flume facility at Chilworth.

15.2.1 Design and Planning

Initial concept generation sessions focused on each major system component, exploring various design and operational approaches. This progressed to detailed design. Upon review and approval of the design proposal, procurement of components and materials commenced, prioritising local suppliers where feasible.

Upon reflection, greater emphasis should have been placed on the complexities associated with the mechanical and electrical design of the powertrain. Consequently, the testing phase experienced multiple setbacks due to failures in this domain. A key finding from the results analysis was a power conversion loss of approximately 50% between mechanical input and electrical output, a figure significantly higher than expected. This discrepancy likely reflects an incomplete initial assessment of suitable generator options, the cost constraints of the project and their integration requirements in the project timeframe.

15.2.2 Assembly and Parallel Development

The physical assembly of the large-scale prototype occurred over several weeks as materials arrived. Design for Manufacture (DFM) principles, a key project requirement, ensured a relatively smooth assembly process despite the considerable size of components like the pontoons. Concurrently, electronic system design and development proceeded. To facilitate seamless integration, a smaller, pre-existing wheel served as a testbed for sensor development. In parallel, the Chilworth flume was characterised across various configurations to establish baseline performance data not previously documented, ensuring precise control of test conditions.

15.2.3 Testing and Iteration

Once assembled, dry testing commenced, including powertrain frictional loss assessments conducted by driving the motor and measuring torque under no-load conditions. Following successful dry tests, the prototype was moved to the outdoor flume for operational testing. While some unforeseen issues arose, requiring minor fixes (typically resolved within 1-2 days with minimal need for new parts),

contingency built into the test plan allowed for the completion of all required tests despite these setbacks.

In retrospect, conducting a more thorough Failure Mode and Effect Analysis (FMEA) could have been beneficial in minimising testing setbacks. A more exhaustive application of this systematic problem identification methodology would likely have highlighted potential issues for earlier resolution.

15.3 Sustainability

The foremost objective of this design is to provide a sustainable power generation solution for rural locations, leveraging existing irrigation canal infrastructure. This technology offers a direct alternative to diesel generators, which are commonly used in such scenarios.

The design refrained from permanent joints where possible, only using glue for the pontoons. The whole of the frame, wheel and powertrain assembly can be broken down to its individual components for reuse, disposal or recycling.

15.4 Communication

Effective communication was paramount to the project's success, encompassing two primary categories. Firstly, inter-team technical communication focused on the clear articulation of design ideas, concepts, and technical details among team members. Secondly, efficient status communication ensured that progress on individual tasks, and any results that might influence decisions by other team members, were promptly shared.

To facilitate these communication flows, a weekly task tracker was implemented. This tool served multiple purposes: it helped individuals maintain focus on their short-term weekly goals, ensured that all activities undertaken contributed tangible value to the project, and prevented duplication of effort. An extract is provided in *Figure 15.1*.

TASK NAME	ASSIGNED TO	DELIVERABLE/ task complete if:	(HRS	STATU	PRIORIT	DEADLINE (If applicabl	Days to deadlin
Sensors/ condition monitor	George	Hall sensor, accelerometer/gyro	5	Complete	Low		
Project initial presentation	Owain	Slides for concepts, irrigation c	5	Complete	Medium	30-Oct	Passed
28 Theory chat	Owain	Email Gerald for discrepancies	2	Complete	<u>High</u>	,	
Decision Matrix	Sam H	Add to literature review	3	In review	<u>High</u>	22-Oct	Passed
20 Parts List	Sam W	Look at suppliers	5	Cancelled	Low		
CAD the Frame	Sam W	Cad that can be reviewed in thu	3	In progress	Medium	24-Oct	Passed
32							
Rough slides interim pres	All	Content	1	Complete	<u>High</u>	24-Oct	Passed
Chilworth inventory	Sam W	Visit Chilworth what aluminium	2	In review	Medium		
Cost benefit analysis	Owain	Wood, vs Ply vs PVC	1	Complete			
36 Highfield RAMS	George	Uploaded to planon	2	Complete			
polish slides	All	Slides finished as best as possi	3	Complete	<u>High</u>	28-Oct	Passed
38 Finish Gantt Chart	Sam H	Update Gantt chart with dates a	3	Complete	<u>High</u>	28-Oct	Passed
39							
Order electro	George	Email Phoebe Links + Costs	1	In review	<u>High</u>	06-Nov	Passed
Order channel mod	Sam W	Email Phoebe Links + Costs	1	In progress	<u>High</u>	07-Nov	Passed
Wainht + Ruovanov calculator	Owein	Come un with a total weight and	5	Not started	Madium	12-Nov	Darrad

Figure 15.1: Extract from the task tracker

16 Further Development

16.1 Closed loop control

To optimise power output, a closed-loop control system is proposed. This system would adjust the generator's electrical load to maintain the wheel at its optimum blade speed, which changes with varying upstream flow conditions. Establishing this requires understanding how the optimum RPM shifts across the operational flow range; therefore, further data collection under diverse conditions is essential.

For dynamic load management, the existing 3-way toggle switches could be upgraded to Arduino interfaced relays. The control logic would then need to determine the target RPM. This could be achieved either through pre-defined calculations if canal flow velocity is accurately known, or through an adaptive approach. In the adaptive method, suitable for stable but less predictable flow, the system would execute an automated sweep (mirroring our current test methodology) to identify and subsequently target the RPM that yields maximum power.

16.2 Electrical ballast release

Observations from tests with the current line-and-plug ballast ejection mechanism indicated a need for enhanced reliability. We propose a future design implementing an electrical ballast release system, utilising a latching solenoid powered by a capacitor. The wheel's own power generation would maintain the capacitor's charge. In an event causing power loss to the wheel, such as a jam, the subsequent power-down of the Arduino microcontroller would initiate a logic sequence to switch the solenoid. This action would open the ballast plugs, forcing ejection. An electrical system can overcome the limitations outlined in section 15.1.3 more effectively than a complex central mechanical release. Additionally, this electronic solution enables remote, preemptive ballast release, for instance, when forecasts predict high rainfall that could reduce available freeboard in the canal.

16.3 Data & monitoring

16.3.1 Data Format Optimisation

To conserve onboard memory resources, the current JSON data format could be transitioned to a more compact Comma-Separated Values (CSV) format for local data logging.

16.3.2 Enhanced Wireless Monitoring

The existing web-based wireless monitoring system will be maintained and potentially expanded to include an app interface, prototyped in *Figure 16.1*. The integration of an Arduino SIM module could be

included to provide cellular data transmission capabilities, enabling remote monitoring even in locations without local Wi-Fi access.

As included in the app, a webcam could be integrated into the system. This feature will allow operators to request and receive a live video feed or still images via the monitoring app, providing visual confirmation of the wheel's status and surrounding conditions.

16.3.3 Predictive Analytics

Data collected from the wheel's sensors could be subjected to advanced processing and pattern recognition algorithms. The aim would be to identify trends and anomalies indicative of potential future maintenance needs (pre-emptive maintenance) or to trigger proactive operational activities.

16.3.4 Industry 4.0 Integration

In alignment with Industry 4.0 concepts, the system could be easily modified to interface with external irrigation management data. This connectivity will enable the waterwheel to respond dynamically to demand, such as ramping power generation up or down based on real-time irrigation requirements, leading to more efficient resource utilisation.

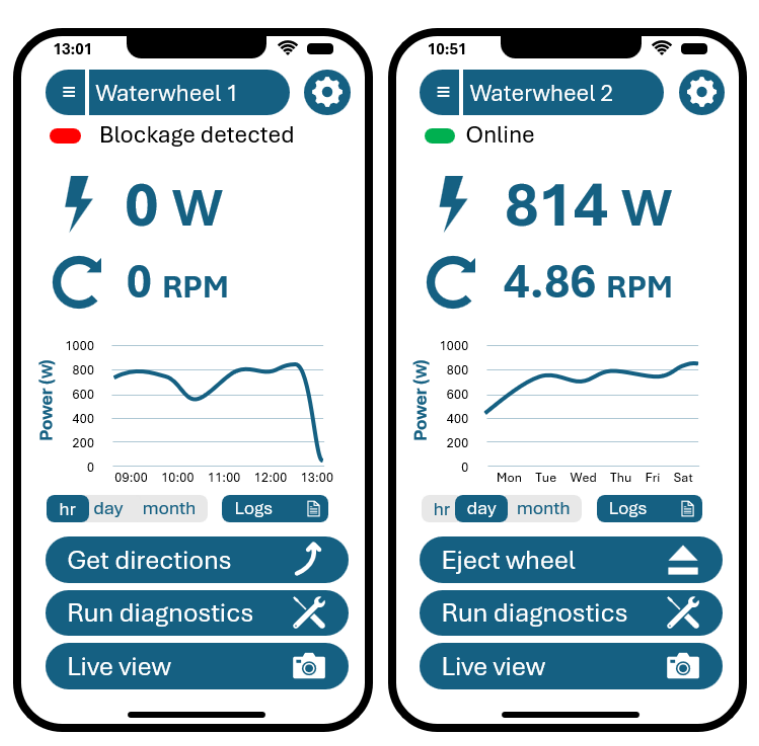


Figure 16.1 - App prototype

16.4 Power conversion

Further investigation is recommended to precisely identify and quantify the primary sources of energy loss within the current powertrain. This analysis should differentiate between various loss mechanisms, such as those occurring in the rectifier circuitry versus resistive losses within the generator windings. Leveraging the insights gained from the initial powertrain development, a subsequent design iteration could then focus on creating a more compact, reliable, and efficient system. The anticipated outcomes of this work include significantly improved overall system efficiency and enhanced operational resilience.

16.5 Pontoon modifications

The current prototype utilises pontoons constructed from XPS foam, coated with a thin silicone layer. This material choice was practical for rapid prototyping, leveraging readily available materials and fabrication tools at the University. However, XPS foam exhibits susceptibility to water absorption and structural weakening when subjected to prolonged exposure to environmental elements. A significant limitation of this design is its poor performance regarding flat-pack shipping, as the solid foam pontoons cannot be disassembled or efficiently packed.

Given these limitations and the expectation that the XPS design would not withstand the final product's operational environment, a more resilient alternative is required. The proposed solution is a blow-moulded plastic pontoon design, conceptualised in *Figure 16.2*. This approach offers superior water resistance over time. The proposal features an open-top design, sealed with a rubber gasket that bolts to the main frame. For transit, the two pontoons could be connected in a clamshell configuration. The internal volume created will then be utilised to securely store all other system components, protecting them during shipping and significantly improving the overall packing efficiency of the design.



Figure 16.2 - Design concept for blow moulded pontoon

As an alternative for lower-volume production runs, where blow-moulding tooling costs may be prohibitive, a hemp-epoxy composite layup could be considered. Using natural hemp fibres aligns with the sustainability goals of the project. This method, drawing inspiration from the marine industry, offers a cost-effective way to produce strong and durable pontoons for smaller, more unique production batches.

17 References

- [1] Soochan, P. (2023) *Food: The 2050 challenge and the women addressing it*. AWIS. Available at: https://awis.org/resource/food-2050-challenge-women-addressing/ (Accessed: 7 May 2025).
- [2] Searchinger, T. et al. (2019) *Creating a sustainable food future: A menu of solutions to feed nearly 10 billion people by 2050*. World Resources Institute.
- [3] Qin, J. et al. (2024) 'Global energy use and carbon emissions from irrigated agriculture', *Nature Communications*, 15(1), p. 3084. doi:10.1038/s41467-024-47383-5.
- [4] Williams, E. (2013) *Impact of increasing energy demands on natural resources*. The Energy Sustainability Challenge. MIT-CSIS.
- [5] Mehta, P. et al. (2024) 'Half of twenty-first century global irrigation expansion has been in water-stressed regions', *Nature*, 8 March. Available at: https://www.nature.com/articles/s44221-024-00206-9 (Accessed: 7 May 2025).
- [6] Horst, M. and J.P.A. (2006) 'Rehabilitation of irrigation systems as an adaptation strategy to climate change in the Aral Sea Basin', *Tropentag 2006: Prosperity and Poverty in a Globalised World*, Bonn, Germany, 11–13 October. Available at:
- https://www.tropentag.de/2006/abstracts/full/211.pdf (Accessed: 7 May 2025).
- [7] Asher, S. et al. (n.d.) 'The long-run development impacts of agricultural productivity gains: Evidence from irrigation canals in India', *VoxDev*. Available at: https://voxdev.org/topic/agriculture/long-run-development-impacts-agricultural-productivity-gains-evidence-irrigation (Accessed: 7 May 2025).
- [8] Fernández García, I. et al. (2020) 'Trends and challenges in irrigation scheduling in the semi-arid area of Spain', *Water*, 12(3), p. 785. doi:10.3390/w12030785.
- [9] Cazcarro, I., Duarte, R. and Sánchez-Chóliz, J. (2013) 'Economic growth and the evolution of water consumption in Spain: A structural decomposition analysis', *Ecological Economics*, 96, pp. 51–61. doi:10.1016/j.ecolecon.2013.09.010.
- [10] Belaud, G. et al. (2019) 'Irrigation and energy: Issues and challenges', *Irrigation and Drainage*, 69(S1), pp. 177–185. doi:10.1002/ird.2343.
- [11] Fader, M. et al. (2016) 'Mediterranean irrigation under climate change: More efficient irrigation needed to compensate for increases in irrigation water requirements', *Hydrology and Earth System Sciences*, 20(2), pp. 953–973. doi:10.5194/hess-20-953-2016.
- [12] Design Council (2025) *The double diamond*. Available at: https://www.designcouncil.org.uk/our-resources/the-double-diamond/ (Accessed: 7 May 2025).
- [13] Zhao, M. et al. (2020) 'Performance investigation of the immersed depth effects on a water wheel using experimental and numerical analyses', *Water*, 12(4), p. 982. doi:10.3390/w12040982.

- [14] Adobe Stock (n.d.) 'Water+Mill images Browse 155,781 stock photos, vectors, and video'. Available at:
- https://stock.adobe.com/uk/search?k=water%2Bmill&asset_id=68230040 (Accessed: 7 May 2025).
- [15] Pujol, T. et al. (2015) 'Hydraulic efficiency of horizontal waterwheels: Laboratory data and CFD study for upgrading a western Himalayan watermill', *Renewable Energy*, 83, pp. 576–586. doi:10.1016/j.renene.2015.04.060.
- [16] Quaranta, E. et al. (2016) 'Optimization of breastshot water wheels performance using different inflow configurations', *Renewable Energy*, 97, pp. 243–251. doi:10.1016/j.renene.2016.05.078.
- [17] Quaranta, E. and Revelli, R. (2020) 'Performance optimization of overshot water wheels at high rotational speeds for hydropower applications', *Journal of Hydraulic Engineering*, 146. doi:10.1061/(ASCE)HY.1943-7900.0001793.
- [18] aQysta B.V. (n.d.) *Barsha Pump: Variants & Technical Specifications*. Available at: https://www.aqysta.com (Accessed: 7 May 2025).
- [19] Dallaev, R. et al. (2023) 'Overview of the current state of flexible solar panels and photovoltaic materials', *Materials*, 16(17), p. 5839. doi:10.3390/ma16175839.
- [20] Glykas, A., Papaioannou, G. and Perissakis, S. (2010) 'Application and cost–benefit analysis of solar hybrid power installation on merchant marine vessels', *Ocean Engineering*, 37(7), pp. 592–602. doi:10.1016/j.oceaneng.2010.01.019.
- [21] Sheikh, Y. et al. (2024) 'Enhancing PV solar panel efficiency through integration with a passive multi-layered PCMS cooling system: A numerical study', *International Journal of Thermofluids*, 23, p. 100748. doi:10.1016/j.ijft.2024.100748.
- [22] Benn, T. (2024) *Building a solar farm: Landowner tips for the construction phase*. Lumify Energy. Available at: https://lumifyenergy.com/blog/building-a-solar-farm/ (Accessed: 7 May

2025).

- [23] Noëth, B. (2025) 'Solar panels blind pilots approaching Amsterdam Schiphol; runway closed for two hours when sunny', *Aviation24.be*. Available at: https://www.aviation24.be/airports/amsterdam-schiphol-ams/solar-panels-blind-pilots-approaching-amsterdam-schiphol-runway-closed-for-two-hours-when-sunny/ (Accessed: 5 May 2025).
- [24] Generator Pro (2025) Warrior 5500 watts silent diesel generator-wireless remote. Available at: https://generator-
- pro.co.uk/product/diesel/warrior-5500-watts-silent-diesel-generator-wireless-remote/ (Accessed: 5 May 2025).
- [25] Matt's Generators (2023) *Off grid power*. Available at: https://mattsgenerators.co.uk/off-grid-power/ (Accessed: 7 May 2025). [26] Rangel, N., Li, H. and Aristidou, P. (2023) 'An optimisation tool for minimising fuel consumption, costs and emissions from Diesel-PV-Battery hybrid microgrids', *Applied Energy*, 335, p. 120748. doi:10.1016/j.apenergy.2023.120748.

- [27] Kirke, B. (2020) 'Hydrokinetic turbines for moderate sized rivers', *Energy for Sustainable Development*, 58, pp. 182–195. doi:10.1016/j.esd.2020.08.003.
- [28] Sarkar, S. et al. (2023) 'Chapter 7 An overview of small-scale hydropower and its recent development', in *Renewable Energy Production and Distribution*. 2nd edn. Academic Press, pp. 249–314. doi:10.1016/B978-0-443-18439-0.00009-4.
- [29] Fox, R.W., Pritchard, P.J. and McDonald, A.T. (2009) *Introduction to fluid mechanics*. 7th edn. Hoboken, N.J.: Wiley. Available at: https://archive.org/details/introductiontofl0000foxr_7ed (Accessed: 4 May 2025).
- [30] Cleynen, O., Engel, S., Hoerner, S. and Thévenin, D. (2021) 'Optimal design for the free-stream water wheel: A two-dimensional study', *Energy*, 214, p. 118880. doi:10.1016/j.energy.2020.118880.
- [31] Hebditch, J. (2024) *Home hydro turbine generator: Can it really power your home?* GivEnergy. Available at: https://givenergy.co.uk/home-hydro-turbine-generator-can-it-really-power-your-home/ (Accessed: 20 January 2025).
- [32] National Grid (n.d.) *Live grid data*. Available at: https://grid.iamkate.com/ (Accessed: 25 April 2025).
- [33] RS Components (2025) *Industrial solutions & electrical components*. Available at: https://uk.rs-online.com/web/ (Accessed: 7 May 2025). [34] PalletOnline (n.d.) *Pallet delivery: Send pallets UK & Europe*. Available at: https://palletonline.co.uk/checkout/ (Accessed: 7 May 2025).
- [35] Brandon-Toole, M., Birzer, C. and Kelso, R. (2023) 'The effect of blade depth ratio on the performance of in-stream water wheels', *Energy for Sustainable Development*, 77, p. 101346. doi:10.1016/j.esd.2023.101346. [36] DripWorks (2024) *Cost-benefit analysis of installing a drip irrigation system*. Available at: https://www.dripworks.com/blog/costbenefit-
- analysis-of-installing-a-drip-irrigation-system (Accessed: 7 May 2025). [37] Chow, V.T. (1959) *Open-channel hydraulics*. New York: McGraw-Hill.
- [38] United States Bureau of Reclamation (USBR) (2001) *Water measurement manual*. 3rd edn. Denver, CO: U.S. Department of the Interior, Bureau of Reclamation. Available at:
- https://www.usbr.gov/tsc/techreferences/mands/wmm.html (Accessed: 4 May 2025).
- [39] Muck, K.C., Hoffmann, P.H. and Bradshaw, P. (1973) 'The effect of convex surface curvature on turbulent boundary layers', *Journal of Fluid Mechanics*, 60(1), pp. 43–62. doi:10.1017/S0022112073000030.

 [40 Zhu, Z. and Wu, X.M. (2024) *Sensorless control of permanent magnet*
- synchronous machine drives. Hoboken, NJ: John Wiley & Sons. doi:10.1002/9781394194384.

18 Appendix

18.1 Appendix A

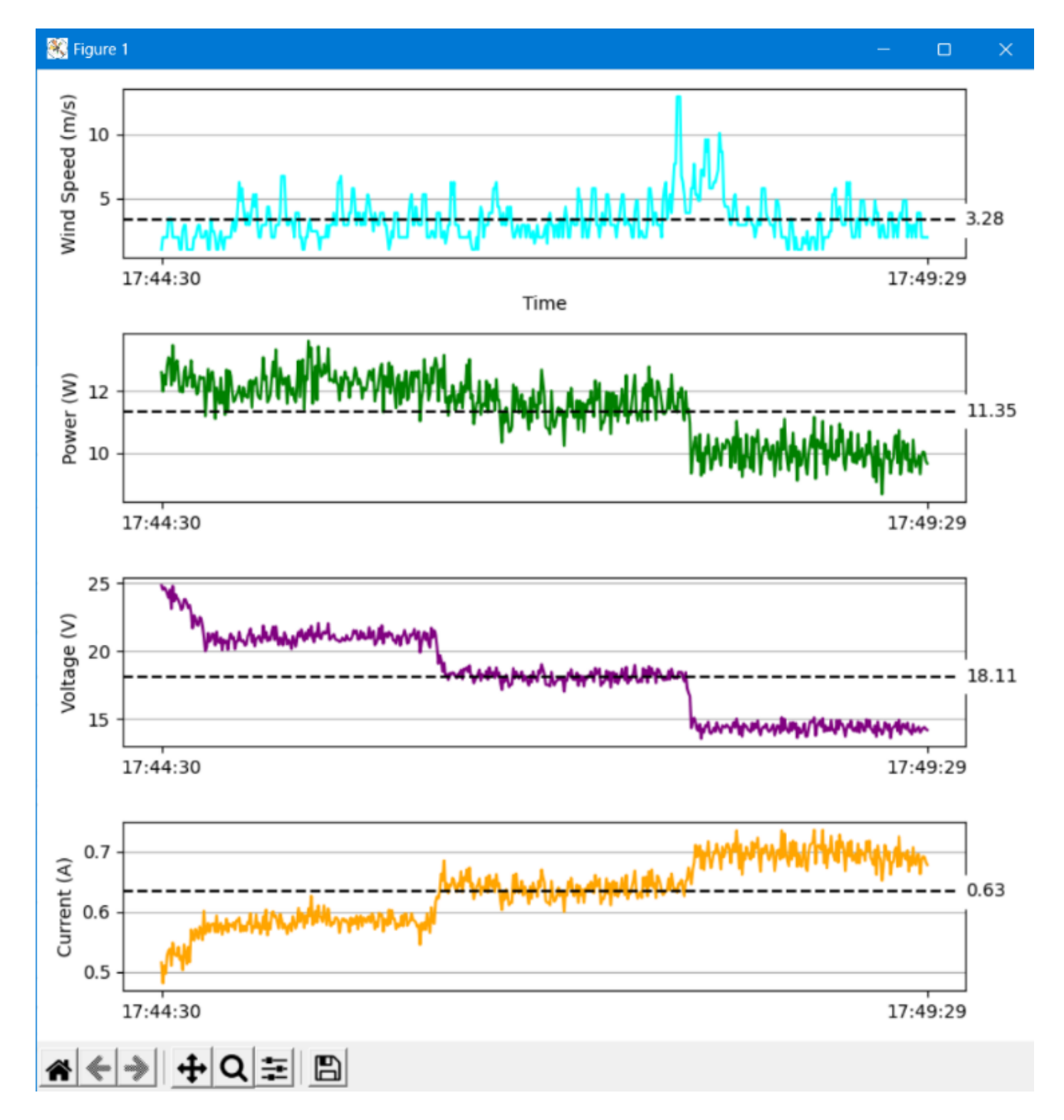


Figure A1 - Screenshot of wireless live plotting graphs

18.2 Appendix B

Location 1

	Pumps configuration	Sluice Gate Height (m)	Channel Depth – IQ [m]	Velocity – IQ [m/s]	Velocity - Stick Test			
Test					Timestamp	Result (m/s)	Comments	
А	1							
Start time:	2							
	3							
В	3							
Start time:	2							
	1							

Location 2

	Pumps configuration	Sluice Gate Height (m)	Channel Depth – IQ [m]	Velocity – IQ [m/s]	Velocity – Stick Test			
Test					Timestamp	Result (m/s)	Comments	
С	1							
Start time:	2							
	3							
D	3							
Start time:	2							
	1							

- Be careful to check that the time on the IQ meter is set correctly.
- Remember to note down the exact time in case the timestamps have an issue like before
- Ensure that the water level with all three pumps on doesn't get too high, it shouldn't but monitor
- . Discuss whether it is better to get two sets of results at the same location or one set of results at different locations in case time is tight.

Figure B1 – IQ Flow test SOP used for example page 1

32

Equipment/Setup Checklist (before anything turned on):

- Check the IQ Z starting position in software, confirm it's right.
- . Some sort of stopwatch can be phone
- Laptop attached to IQ and charger (if needed)
- Metre rule place long aluminium extrusion across channel horizontally tape metre rule to midpoint vertically to measure depth or use bridge
- IQ is in flume and plugged in weights keeping it down will need power can be run from the main green box at far end of flume
- Have a stick collection (need 12) to use for stick test and mark out specific distance that will be used to measure stick test, decide on these before turning flume

Step	Tick Box
1) Place IQ flow sensor into canal location 1 using weights, (either tape of weigh down cable too), start measurement recording and	
mark down the exact time of experiment start time. Ensure the IQ is giving out readings.	
2) Adjust sluice gate so that it is approx. halfway down, will need to be moved so only rough will do	
3) TURN ON a single pump and wait 5 minutes	
4) Using the metre rule measure the depth at location X, adjust the sluice gate height so that the depth measures 0.4m. (or as close as	
possible)	
5) Once the depth reaches 0.4m measure the height of the sluice gate using a metre rule.	
6) Measure velocity values:	
a) Using the instant reading on the IQ display, get this value at the start time of the stick test.	
b) Stick test - set distance and measure time - (speed = distance / time) - record in table along with the timestamp it was started at	
7) Lower sluice gate to approx. halfway again and TURN ON second pump. Monitor water level, two pumps should be on. – WAIT FIVE	
MINUTES	
8) Repeat steps 4-6	
9) Lower sluice gate to fully open and TURN ON third pump. Again, monitor water level, three pumps should be on. – WAIT FIVE	
MINUTES	
10) Repeat steps 4-6	
11) Wait 5 minutes	
12) Repeat steps 4-6, you should now have two sets of measurements for the <u>3 pump</u> scenario	
13) TURN OFF the third pump (2 pumps shown be on now) - WAIT 5 MINUTES - repeat Steps 4 and 5, you should now have two sets of	
measurements for the 2 pump scenario	
14) TURN OFF the second pump (1 pump shown be on now) - WAIT 5 MINUTES - repeat Steps 4 and 5, you should now have two sets of	
measurements for the 1 pump scenario	
15) Make sure you have six sets of measurements then TURN OFF last pump (no pumps on now) – allow flume to empty	
16) Repeat all steps for location 2	

Figure B2 – IQ Flow test SOP used for example page 2

18.3 Appendix C

Table C1 – Financial summary

Item Name	Cost-code	Quantity	Price	Delivery	Total Cost
Arduino	510667101	1	£ 16.60	£ 2.00	£ 18.60
IMU	510667101	1	£ 19.72	£ 2.00	£ 21.72
Hall Effect Sensor	510667101	1	£ 5.73	£ 2.00	£ 7.73
Current + Voltage Sensor	510667101	1	£ 7.86	£ 2.00	£ 9.86
Arduino Header	510667101	4	£ 1.68	£ 2.00	£ 8.72
Protoboard	510667101	2	£ 2.49	£ 2.00	£ 6.98
PVC	510667101	1	£ 149.70	£ 21.00	£ 170.70
Aluminium Extrusions	510667101	9	£ 18.29	£ 18.60	£ 183.21
Pressure Treated Fence Post	510667105	4	£ 12.00	£ 6.00	£ 54.00
Marine Ply Sheets	510667105	2	£ 53.94	£ 13.49	£ 121.37
Far Eastern Plywood Sheets	510667105	2	£ 38.16	£ 9.53	£ 85.85
Foam	510667101	1	£ 98.83	£ -	£ 98.83
Aluminium Extrusions (total order or varying lengths)	514682101	1	£ 150.05	£ 18.60	£ 168.65
Aluminium Angle Bar	514682101	1	£ 61.34	£ 18.60	£ 79.94
Central Shaft Aluminium and Aluminium round bar	514682101	1	£ 61.34	£ -	£ 61.34
MOT-I-81491-L	510667101	1	£ 305.22	£ 69.70	£ 374.92
Timing Belt	514682101	1	£ 38.05	£ -	£ 38.05
150mm diameter timing pulley	514682101	1	£ 60.00	£ 2.25	£ 62.25
50mm diameter two groove pulley	514682101	1	£ 13.42	£ -	£ 13.42
2012 50mm Taperlock Bush	510667105	1	£ 6.55	£ -	£ 6.55
1008 12mm Taperlock Bush	510667105	1	£ 3.70	£ -	£ 3.70
1 Mod, 120 tooth metric spur gear in steel, 12mm bore diameter, 2x grub screws	510667105	1	£ 65.09	£ -	£ 65.09
1 Mod, 24 tooth metric spur gear in steel, 12mm bore diameter, 2x grub screws	510667105	1	£ 21.89	£ -	£ 21.89
SPZ150-2-2012 V Belt Pulley Wheel	510667105	1	£ 20.44	£ -	£ 20.44
SPZ50-2-1008 V Belt Pulley Wheel	510667105	1	£ 10.26	£ -	£ 10.26
Z79 (10x2007 Li) V Belt	510667105	1	£ 4.86	£ -	£ 4.86
Individual Claim Form (motor controller)	514682101	1	£ 27.98	£ -	£ 27.98
Central Hubs EDMC	514682101	1	£ 15.00	£ -	£ 15.00
Powertrain baseplate	514682101	1	£ 20.00	£ -	£ 20.00
					£ 1,781.91